Diffusion Tensor Imaging and Tractography of the Visual Pathways

Ylva Lilja

Department of Clinical Neuroscience
Institute of Neuroscience and Physiology
Sahlgrenska Academy at University of Gothenburg

UNIVERSITY OF GOTHENBURG

Gothenburg 2016

Cover illustration: 3D tractography of the visual pathways, by Ylva Lilja

Diffusion Tensor Imaging and Tractography of the Visual Pathways

ylva.lilja@neuro.gu.se

ISBN 978-91-628-9870-0 (PRINT), http://hdl.handle.net/2077/43459
http://hdl.handle.net/2077/43459

Printed in Gothenburg, Sweden 2016
Printed by Ineko AB, Gothenburg

ABSTRACT

The visual pathways are essential for human vision, stretching from the retinas of the eyes, via the anterior visual pathways and the optic radiations, to the primary visual cortex in the occipital lobe. Injury to these structures will lead to visual impairment – from small deficits to blindness. Diffusion tensor imaging (DTI) can be used to assess nervous pathways in the brain, non-invasively and *in vivo*. Diffusion properties, measured by DTI, have been shown to correspond to pathology in nervous tissue and, furthermore, can be used for visualization of white matter tracts through *tractography*.

Temporal lobe resection (TLR) may be indicated for medically refractory temporal lobe epilepsy or tumors. During TLR the optic radiation (OR) may be surgically injured, which may lead to significant visual field defects (VFD). The aim of study I and II, was to assess the anatomical accuracy of tractography of the OR and, ultimately, the use of tractography for surgical guidance in order to reduce postoperative VFDs. Two different tractography algorithms were assessed: deterministic (DTG) and probabilistic tractography (PTG).

In Study I, PTG and DTG of the OR were performed in 23 DTI scans (46 ORs). The anterior extents of the OR tractographies were measured. Results by PTG placed the OR more anteriorly and were the closest match to dissection studies and to a histological atlas. The aim of Study II was to validate the individual anatomical accuracy of OR tractographies from eight patients who underwent TLR. The results showed that the postoperative degree of VFD could be predicted based on the preoperative OR tractography and the resection size.

In conclusion, PTG is a strong candidate for surgical guidance of TLR that aims to minimize injury to the OR.

Pituitary adenomas may cause visual impairment by compression of the anterior visual pathways. Early detection of injury is crucial in order to initiate treatment while it is reversible. DTI may be used as a diagnostic tool of early injury, however, the anterior visual pathways, including the optic tracts, represent challenging structures for DTI analysis.

The aim of Study III was to assess different DTI-data extraction methods of the optic tracts and to find a reliable method, defined as a method with low method-dependent variability and high anatomical accuracy. Four region-of-interest (ROI) methods were compared, out of which three could be found in

previous literature and one was new, based on the FA-skeleton algorithm of tract-based spatial statistics (TBSS). DTI measures by the four methods were significantly different and the semi-automatic method based on the FA-skeleton proved to perform best.

The aim of Study IV was to assess the value of DTI as an objective diagnostic tool for injury of the anterior visual pathways in patients with pituitary adenomas. The FA-skeleton ROI method was applied on DTI scans of 23 patients who underwent surgery for pituitary adenomas. DTI measures proved to correlate with the degree of VFD and to differ significantly between patients and controls, which may correspond to levels of demyelination and axonal atrophy in the patient group.

In conclusion, DTI could detect pathology and degree of injury in the anterior visual pathways and may be useful as an objective diagnostic tool for patients with pituitary adenomas. Choice of ROI method was found to be highly influential on DTI measures when the optic tracts were analyzed.

Keywords: Diffusion tensor imaging, Tractography, Visual pathways, Meyer's loop, Temporal lobe resection, Anterior visual pathways, Pituitary adenoma

ISBN: 978-91-628-9870-0 (PRINT), http://hdl.handle.net/2077/43459

LIST OF PAPERS

This thesis is based on the following studies, referred to in the text by their Roman numerals.

I. Visualizing Meyer's Loop: A Comparison of Deterministic and Probabilistic Tractography

Lilja Y, Ljungberg M, Starck G, Malmgren K, Rydenhag B, Nilsson D

Epilepsy Research: 2014, Mars; 108(3): 481-90

II. Tractography of Meyer's loop for temporal lobe resection – validation by prediction of post-operative visual field outcome

Lilja Y, Ljungberg M, Starck G, Malmgren K, Rydenhag B, Nilsson D

Acta Neurochirurgica (Wien): 2015 Jun; 157(6): 947-56

III. Impact of region-of-interest method on quantitative analysis of DTI data in the optic tracts

Lilja Y, Gustafsson O, Ljungberg M, Nilsson D, Starck G

BMC Medical Imaging: 2016 Jul 11; 16(1): 42

IV. Visual-pathway impairment by pituitary adenomas – quantitative diagnostics by diffusion tensor imaging

Lilja Y, Gustafsson O, Ljungberg M, Starck G, Lindblom B, Skoglund T, Bergquist H, Jakobsson K-E, Nilsson D

In press: Journal of Neurosurgery DOI: 10.3171/2016.8.JNS161290

CONTENT

ABBREVIATIONS

CSD	Constrained spherical deconvolution
CSF	Cerebrospinal fluid
DTG	Deterministic tractography
DTI	Diffusion tensor imaging
DWI	Diffusion weighted imaging
FA	Fractional anisotropy
LGN	Lateral geniculate body
MD	Mean diffusivity
MRI	Magnetic resonance imaging
OCT	Optical coherence tomography
OT	Optic tract
PTG	Probabilistic tractography
RNFL	Retinal nerve fiber layer
ROI	Region of interest
SIPAP	Suprasellar, infrasellar, parasellar, anterior and posterior
TBSS	Tract-Based Spatial Statistics
TLR	Temporal lobe resection
TP-ML	Distance between the temporal pole and the anterior limit of Meyer's loop
VBM	Voxel-based morphometry
VFD	Visual field defect

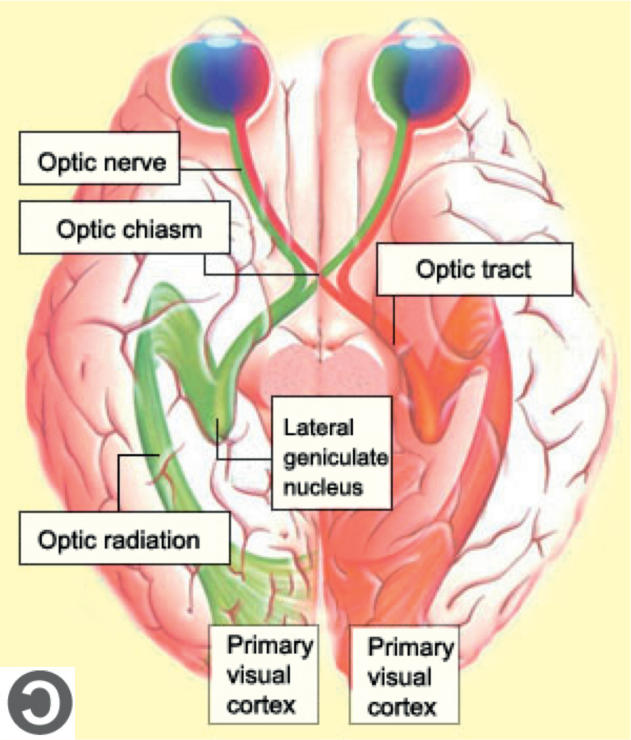

Figure 1. The visual pathways of the brain. Copyleft at http://thebrain.mcgill.ca.

INTRODUCTION

The visual pathways are essential structures for human vision, linking the eyes with the visual cortex in the brain. As the visual pathways extend throughout the whole of the brain, in a front to back direction, they can be subject to injury due to lesions with several different locations. Such localized injury can for example be caused by tumors or trauma, including surgical trauma. Injury of the visual pathways will lead to varying degrees of visual impairment and, in the most severe cases, to complete loss of vision.

Reliable clinical diagnostic tools are crucial for a successful treatment. Diffusion tensor imaging (DTI) is a magnetic resonance imaging (MRI) technique with a unique ability to visualize and assess nervous pathways in the brain, including the visual pathways. This thesis aims to explore the ability of DTI to provide valuable information about the visual pathways in two specific clinical conditions: first, patients planned for surgery in the temporal lobes, with the aim to prevent visual impairment caused by surgical trauma and, second, patients with large pituitary tumors, with the aim to objectively diagnose injury to the visual pathways.

1.1 The visual pathways

The visual pathways are a complex circuitry that is part of the central nervous system. The pathways convey and organize visual information from the eyes to different centers in the brain that provide visual perception as well as control several non-image photo-response functions.

The anterior visual pathways start at the retinas of the eyes and terminate in nuclei of the thalamus and the midbrain (Figure 1). Axons from the ganglion cells of the retinas pass through the wall of the eyeball at the optic papilla. They then form the optic nerves, which pass through the orbits and enter the cranial cavity. Here, the optic nerves cross over in the optic chiasm and continue posteriorly as the optic tracts. A minority of the neurons of the optic tracts project to the midbrain, which corresponds to the non-image photo-response functions, such as control of the pupillary reflex and the circadian rhythm. The majority of the optic tract neurons terminate in the lateral geniculate nuclei (LGN) of the thalamus. From the LGN the visual pathways continue as the optic radiations via the temporal and parietal lobes to the cerebral cortex in the occipital lobe – the primary visual cortex [18].

An optic nerve contains about 770 000 to 1.7 million myelinated axons [53]. The thickness of the axons varies, but the majority has a diameter of around 0.7 μm. In other words, a cross section of an optic nerve consists of several hundred thousand axons per mm^2.

Throughout the visual pathways there is a strict organization of nerve fibers corresponding to specific areas of the retinas, and thus specific parts of the visual fields – i.e. a retinotopic organization. The optic nerves carry information from each corresponding eye. In the optic chiasm there is a reorganization: fibers corresponding to the lateral visual fields of each eye cross over to the contralateral side while fibers corresponding to the nasal visual fields do not cross over. As a result, each optic tract contains fibers that carry information from the contralateral hemifield of both eyes. In other words, from the optic tracts and onwards, visual information from the right hemifields is conveyed by fibers of the left side of the pathways, and vice versa.

The optic radiations first project out from the LGN as a compact bundle and then quickly fan out in divisions, each representing different parts of the hemifields [66]. The superior bundles primarily contain fibers corresponding to the lower half of the contralateral hemifield and the inferior bundles contain fibers corresponding to the upper half of the contralateral hemifield.

Due to the retinotopic organization of the visual pathways, a localized injury – such as a compressing tumor or a traumatic injury - will lead to a visual field loss with a specific pattern. For example, tumor compression of the central portion of the optic chiasm will eventually lead to a bitemporal hemianopia (Figure 2), as the affected fibers carry information from the lateral visual fields of both eyes. Also, a complete injury of the lower projections of an optic radiation, for example as a complication to surgery, will lead to a contralateral homonymous superior quadrantanopia (Figure 2).

Visual field examination

The visual field is the portion of space that is visible during steady fixation of the gaze in one specific direction. Visual field examination, or *perimetry*, is the systematic measurement of the visual field function.

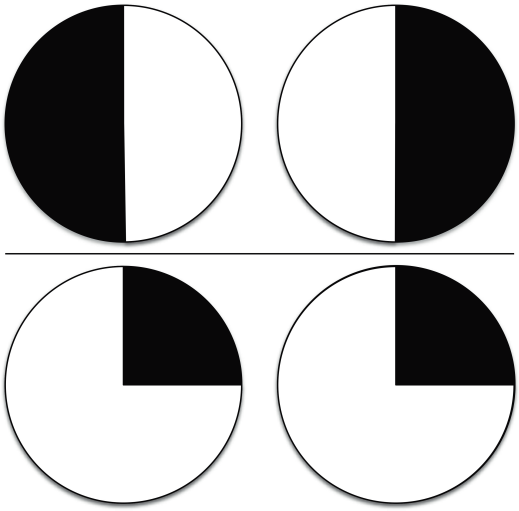

Figure 2. Two cases of visual field impairment. The areas of the visual fields lost in each eye are shown in black. Upper row: bitemporal hemianopia. Lower row: right homonymous superior quadrantanopia.

Perimetry can be manual or automated. Goldmann perimetry is the most common manual test. With Goldmann perimetry, a trained operator moves a stimulus into the visual field. The subject signals when the stimulus is visible and thus the limits of the visual field can be mapped. With automated perimetry, a computer program is used, which typically presents static stimuli (or *targets*) at different locations within a subject's expected visual field, and the subject signals when a target is visible. High-pass resolution perimetry, represented in this thesis, is one kind of static automated perimetry [40].

Visual field examination is important in diagnosing diseases of the visual pathways; the test is sensitive to early signs of pathology and specific patterns of visual field loss can reveal specific pathology and/or locations of injury. However, both manual and automated tests are dependent on the cooperation and response of the patient and are thus both subjective with relatively large reference intervals, which must be considered in their interpretation.

1.2 Diffusion tensor imaging

Brownian motion, or molecular diffusion is the random displacement of molecules in a fluid, as the molecules are agitated by thermal energy. The phenomenon is named after botanist Robert Brown who, in 1827, observed and described the spontaneous motion of pollen grains dispersed in water [19]. In the early 20th century, Albert Einstein revisited the phenomenon and published a paper that explained in detail how the motion that Brown had observed was the result of pollen being moved by individual water molecules [35].

In the human body, water is the dominating diffusing molecule and its displacement is random as long as the medium is homogenous and there are no barriers, such as in the ventricles in the brain. However, biological tissue is often highly heterogeneous media consisting of boundaries that will hinder the mobility of water molecules, such as cell membranes, organelles and other macromolecular structures. Thus, the diffusivity is affected and the displacement is no longer random – a fact that is exploited in diffusion MRI.

The image acquisition of diffusion MRI is based on a specific pulse sequence called pulsed gradient spin echo, first introduced by Stejskal and Tanner in 1965 [93]. The principle behind this sequence is the application of bipolar magnetic gradients; the first gradient pulse dephases and the second pulse rephases the magnetization of protons in a specific volume element (i.e. *voxel*). For stationary elements, such as macromolecules, the pulses induced by both gradients will cancel out. However, for non-stationary particles, such as diffusing water molecules, some of them will have moved between the pulses. As a consequence, the rephasing will be incomplete and signal will be lost. The magnitude of signal loss is thus an indirect measure of water diffusivity in the tissue.

For diffusion-weighted imaging (DWI), introduced in the 1980s, three orthogonal diffusion gradients are applied. The result is images that can visualize the mean diffusivity of tissues, which may be useful for the detection of pathological conditions where the distribution of water is altered, such as for early detection of stroke [70].

While examining the brain with DWI it was discovered that, in gray tissue, the mean diffusivity was independent of the diffusion gradients' directions whilst it would differ depending on directions in white matter. Moseley et al. (1990) carried out the first systemic study based on this observation and concluded that the diffusion of water is isotropic in gray matter (i.e. equal in

all directions), but anisotropic in white matter (i.e. expressing a principal diffusion direction) [71]. The anisotropic diffusion in white matter is due to the parallel organization of axons, where water diffusion is hindered perpendicular to the axons but allowed to move more freely along the direction of the axons. This finding lead to the development of DTI, which measures the anisotropic diffusion in order to visualize and assess the nervous pathways [4,5].

Since the introduction of DTI in the 1990s, there has been a great scientific interest in the technique and its possibilities to further our knowledge of the physiology and pathology of the brain. Clinical research is currently being conducted alongside with continuous improvements of the DTI technique. Some discoveries have lead to the introduction of DTI as a clinical tool, such as the visualization of white matter pathways for neurosurgical guidance [69,72,75,76].

Diffusion tensor imaging (DTI)

- A non-invasive, *in vivo* MRI technique.
- Detects the size and direction of water diffusion.
- As diffusion is larger parallel to axons and hindered perpendicular to axons…
- …DTI can provide information about the location and integrity of white matter pathways.

1.2.1 The tensor in DTI

In contrast to the three magnetic field gradient directions of DWI, six or more gradient directions are required for DTI, which allows for the computation of not only the mean diffusivity but also the magnitudes of diffusivities in different directions. The diffusion pattern of a voxel is illustrated as a tensor, based on three orthogonal principal eigenvectors that are ordered by the magnitudes of their corresponding eigenvalues, i.e. $\lambda_1 > \lambda_2 > \lambda_3$ (Figure 3).

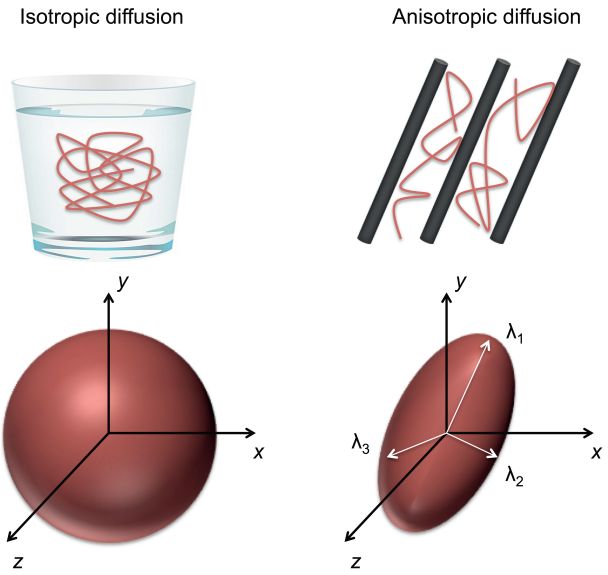

Figure 3. Diffusion. Left: Isotropic diffusion = equal diffusion in all directions, illustrated as a sphere. Right: Anisotropic diffusion = a principal diffusion direction (λ_1) and smaller perpendicular diffusivities (λ_2 and λ_3), illustrated as a tensor.

The magnitude of the principal diffusion direction, λ_1, corresponds to diffusion parallel to the axons: λ_1 = *axial diffusivity*.

The mean of λ_2 and λ_3 corresponds to diffusion perpendicular to the axons: ($\lambda_2 + \lambda_3$)/2 = *radial diffusivity*.

The mean of all eigenvalues corresponds to the mean diffusivity: ($\lambda_1 + \lambda_2 + \lambda_3$)/3 = *mean diffusivity* (MD)

Fractional anisotropy (FA) is a measure of the level of anisotropy on a scale from 0 to 1:

$$FA = \sqrt{\frac{3}{2}} \frac{\sqrt{(\lambda 1 - \mathrm{MD})^2 + (\lambda 2 - \mathrm{MD})^2 + (\lambda 3 - \mathrm{MD})^2}}{\sqrt{\lambda_1^2 + \lambda_2^2 + \lambda_3^2}}$$

1.2.2 The biological basis of diffusion anisotropy

Following the observation that water diffusion is greater parallel to the direction of white matter pathways, the question follows: Which microscopic structures and/or physiological processes contribute to the anisotropy and influence the specific DTI measures? Several studies have explored this by examining the role of myelin, the axonal membranes and the structures of the intracellular compartment (Figure 4).

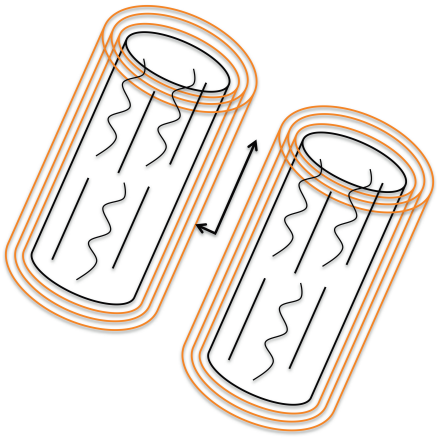

Figure 4. Schematic illustration of sections of two axons: the myelin sheaths (orange layers), the axonal walls (black cylinders) and the cytoskeleton (inner lines and waves). The arrows indicate the extracellular anisotropic diffusion. Long arrow = axial diffusivity; short arrow = radial diffusivity.

The water impermeable lipid layers of myelin may initially be thought to be an important source of anisotropic diffusion. However, studies on non-myelinated nerves – naturally occurring in garfish and induced in mouse and rat models - have shown that the external structural features of the axons, i.e. the axonal membranes, are sufficient to give rise to anisotropy. The studies further conclude that the radial diffusivity will increase with demyelination, along with constant axial diffusivity and decreased, but still present anisotropy. Thus, the degree of myelination will modulate the anisotropy. Furthermore, the axial diffusivity has been shown to decrease with axonal degeneration, along with little change in radial diffusivity [8,44,91,92,114].

The parallel organization of the axonal cytoskeleton – the neurofilaments and the microtubules – may be thought to affect the anisotropy, as well as the longitudinally directed fast axonal transport. However, Beaulieu and Allen (1994) studied the role of the cytoskeleton in garfish nerves with depolymerized microtubules and inhibited fast axonal transport and could observe a preserved anisotropy [8]. Furthermore, giant axons of squid and lamprey enabled studies that measured diffusivity in the intracellular compartment exclusively; it was observed that when water was restricted only by the matrix of neurofilaments, the diffusion was essentially isotropic [9,96].

In conclusion, by systematically assessing the role of intra- and extracellular structures, it was confirmed that intact axonal membranes are the primary determinant of anisotropic water diffusion in white matter pathways [7].

1.2.3 Diffusion tensor tractography

Tractography is the visualization of white matter tracts that can be derived based on the tensor information provided by DTI [6,25,67]. The underlying assumption is that the principal diffusion direction is aligned with the direction of the axons. By connecting voxels based on their principal diffusion direction and their levels of anisotropy, images of white matter pathways can be constructed. Tractography has important clinical applications in neurosurgery, including preoperative planning and intraoperative guidance [72,75,76]. Furthermore, tractography can be used to identify regions-of-interest in white matter, for subsequent extraction and analysis of diffusion measures.

Tractography can be carried out through different mathematical algorithms that consider and include the tensor information in different ways. Advantages and disadvantages can be argued for most such algorithms as tractography presents several challenges. First, the voxel size of a DTI scan is much larger than the axons and the space between axons that is being studied; a regular voxel of 1-2 mm in each dimension will contain several hundred thousand axons. Thus, within a specific voxel there may be part of more than one white matter pathway, with different directions (crossing or “kissing” pathways), as well as change in direction (curving) of a specific pathway. Tractography algorithms deal with these challenges to different extents and in different ways. Methodological research is presently ongoing in this field, with the aim to find models that fit the microstructural reality.

1.3 Temporal lobe resection and visual deficits

1.3.1 Temporal lobe resection

Temporal lobe resection (TLR) may be indicated at several conditions, including medically resistant epileptogenic foci and tumors in the temporal lobe. In the case of temporal lobe epilepsy, more than one third of the patients are resistant to drug therapy [88]. TLR is a well-established treatment for this group, resulting in a high frequency of sustainable seizure freedom with low morbidity [13,108]. However, 50 to 90 % of patients with temporal lobe epilepsy who undergo TLR suffer a post-operative visual field defect (VFD), due to injury to the most anterior part of the optic radiation, Meyer's loop [34,73]. A large enough VFD due to TLR can lead to ineligibility to drive, which is reported to afflict 4 to 50% of patients despite of being seizure free [14,50,65,79]. Evaluations have shown that the ability to drive is one of the most important life-quality goals for patients who consider epilepsy surgery [14,98].

Meyer's loop is located in the anterior part of the temporal lobe, adjacent to other white matter pathways. It cannot be visually separated from other white matter structures by the surgeon's eyes, or by conventional imaging techniques. However, with advances in fiber tractography by DTI, Meyer's loop can be visualized *in vivo*. Accurate delineation of Meyer's loop with tractography may be used for TLR in order to assess the risk of a postoperative VFD as well as for intraoperative guidance.

1.3.2 Meyer's loop

The anterior bundle of the optic radiation that forms Meyer's loop was first identified in 1906 by Archambault and later described more in detail by Meyer in 1907 [2,66]. It extends anteriorly in the temporal lobe, spreading out in a thin sheet of fibers and turning sharply in a bend around the roof of the temporal horn of the lateral ventricle, before continuing posteriorly towards the occipital lobe. The anterior bundle, including Meyer's loop, represents the superior quadrant of the contralateral visual field, and thus a complete injury to the structure during surgery results in a superior contralateral quadrantanopia (Figure 2)[47,66].

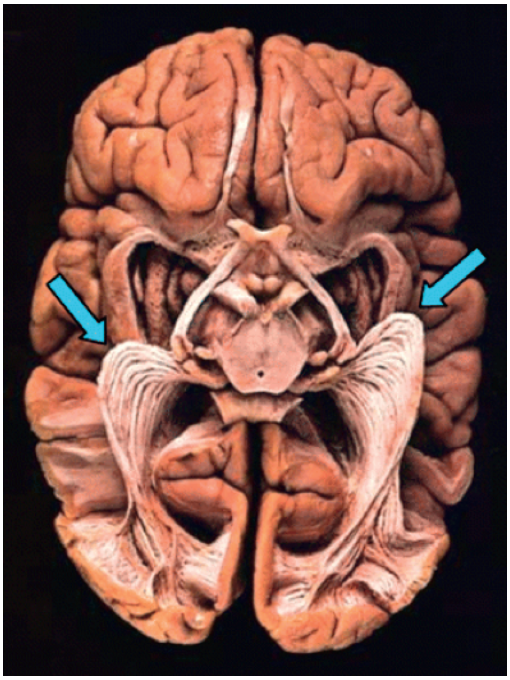

Figure 5. The optic radiation exposed (virtual hospital). A brain seen from below, prepared using Klingler's fiber dissection technique. The arrows indicate Meyer's loop.

The architecture of the optic radiation has primarily been explored and determined by dissection studies using Klingler's fiber dissection technique (Figure 5) [63]. Ebeling and Reulen (1988) dissected 25 brains and presented a distance between the temporal pole and the anterior limit of Meyer's loop (TP-ML) of 27 mm (range 22-37 mm) [32]. Other dissection studies have found similar results and have also confirmed the considerable interindividual variation of the anterior extent of Meyer's loop (Table 1) [24,82,85]. Furthermore, studies have shown an interhemispheric asymmetry of the anterior extent of Meyer's loop with a more anterior location in the left temporal lobe [30,50]. This difference has been proposed to be due to expanding language areas in the posterior part of the left temporal lobe, displacing Meyer's loop forwards on this side.

Based on the variability in location of Meyer's loop, a general safety limit for avoiding injury to the structure during TLR is difficult to specify and individualized methods are required in order to achieve this goal.

Meyer's loop

- The most anterior aspect of the optic radiation in the temporal lobe.
- Represents fibers of the superior quadrants of the contralateral visual fields.
- Significant interindividual and interhemispheric variation of the anterior extent.
- Bends around the roof of the temporal horn of the lateral ventricle as a thin sheet of fibers.

1.3.3 Tractography of Meyer's loop

Meyer's loop is a challenging structure for tractography due to its location in close vicinity to other white matter tracts and its thin and sharply bending shape, leading to a high likelihood of voxels with kissing, crossing and curving fibers. Nevertheless, several tractography studies have successfully visualized Meyer's loop (Table 1) [1,16,23,30,31,49,62,74,89,97,110,112,115,117]. All studies confirm the inter-individual difference of the anterior extent of Meyer's loop in the temporal lobe, also found in dissection studies. However, the mean and range of the anterior extent differ between studies, as well as several of the variables in the tractography acquisitions; some of which seem to have a significant effect on the final tractography delineations.

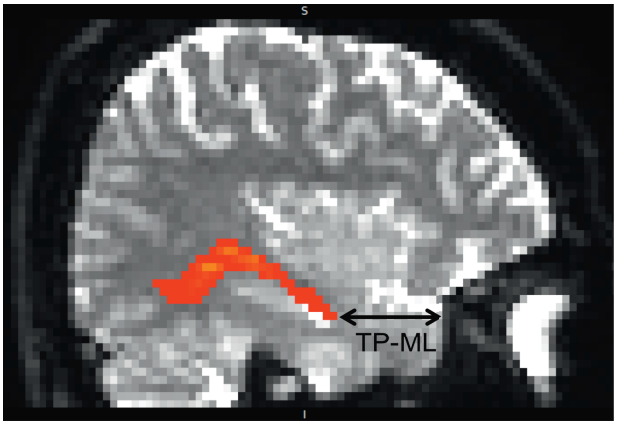

Figure 6. Sagittal image of a brain, including a tractography of the optic radiation (red). TP-ML = the distance between the temporal pole and the anterior limit of Meyer's loop, measured as demonstrated with arrow.

The measurement in focus of these studies is most often the distance between the temporal pole and the anterior limit of Meyer's loop (TP-ML) (Figure 6). Although other shape and location qualities may be of interest, TP-ML may be considered the most important measure intraoperatively, since the most anterior part of Meyer's loop is most prone to injury during TLR. Also, the specific qualities of the anterior-most part makes it the most challenging for tractogrpahy and it may thus be an indicator of success of the tractography as a whole.

To this date, most clinical studies that have explored the accuracy of Meyer's-loop delineation by tractography have used either deterministic (DTG) or probabilistic tractography (PTG).

In DTG, the orientation within a voxel is assumed to be precisely known. A tract is produced by defining a start point and applying an algorithm linking voxels with similar diffusion directions. The technique can be refined by applying threshold criteria, such as a minimum FA-value and a maximum angle of deviation of principal diffusion direction between voxels. Multiple regions of interest are defined, to specify where the tract must pass, a technique known as "virtual fiber dissection" [21]. The advantages of DTG are relatively fast and simple calculations with a clear delineation of fiber tracts. The main limitations are operator-dependency, difficulties resolving curving,

crossing or kissing tracts and no indication of the confidence that one can assign to a reconstructed trajectory [54].

In contrast to DTG, PTG calculates the uncertainty of diffusion orientation within each voxel. It then traces a large number of possible pathways (typically >5000) from a set starting point [54]. The result is a probability distribution of connections and, by selecting an appropriate threshold below which connections are discarded as unlikely, tracts can be outlined. PTG is less likely to exclude voxels with low FA due to, for example, crossing fibers or scan artifacts. However, PTG requires long calculation times, may lead to false positive results [58] and, furthermore, the algorithm is not as widely supported by the MRI scanner manufacturers' own software as is DTG. Thus, third party software is required for PTG, which adds complexity to the tractography process.

1.4 Pituitary adenomas and the anterior visual pathways

1.4.1 DTI of the anterior visual pathways

The anterior visual pathways are relatively small but easily distinguishable structures in MR images, including DTI, as they are surrounded mostly by CSF and the sphenoidal bone. Furthermore, both the macro- and microstructural anatomy is well known, with the retinotopic organization of axons including the crossing over of fibers in the optic chiasm.

Several clinical group-comparison studies have demonstrated the ability of DTI to detect pathological microstructural changes in the anterior visual pathways. The majority of these studies have focused on conditions where the anatomy of the pathways remains largely unchanged, such as optic neuritis and glaucoma [28,103,114,118]. For example, Dasenbrock et al (2011) compared DTI measures in the optic tracts of a control group and 23 patients with multiple sclerosis. They found a higher radial diffusivity in the patient group, which could correspond to demyelination, and that a lower optic-tract FA was correlated to thinning of the retinal nerve fiber layer [28]. Zhang et al (2012) assessed DTI measures of the optic nerves in patients with normal-pressure glaucoma and an age-matched control group and found a significantly lower FA in the glaucoma group [118].

1.4.2 Challenges of DTI-data extraction

To this date, there is no consensus about normal values of DTI measures. A group comparison may thus reveal differences in DTI measures, but DTI measurements from a single individual are difficult to evaluate. Furthermore, there is yet no consensus about the methodology of DTI-data acquisition, although previous studies have reported a variability of DTI measures due to several non-physiological factors, such as scanner-specific factors [17,43,64,104], parameters of the MRI protocol [12,107], selected method for raw data post processing and of data extraction [15,43,45,90]. Previous work has also reported a higher variability of DTI measures extracted from small structures, such as the anterior visual pathways, compared to those of larger structures [17,45,56,60,77,105]. Awareness of these methodological effects and differences due to structure qualities are important in the design of DTI-acquisition protocols and care should be taken when comparing results from differing DTI acquisitions, as different results could be due to the imaging process itself.

Although the anterior visual pathways can be clearly visualized by DTI, the quantitative assessment of diffusion measures in these structures present challenges. The normal dimensions are relatively small (height x width): optic tracts 2.8 x 5.1 mm; nerves 3.0 x 5.9 mm; chiasm 3.5 x 15.0 mm [78]. Pathological conditions in the structures, such as external compression, can lead to even smaller dimensions. As the normal resolution of a clinical DTI scan is around 2 mm per voxel side, there is a substantial risk of partial volume effect, where inclusion of diffusion values from the surrounding CSF will decrease the mean anisotropy of the voxels. Furthermore, due to the crossing of axons in the chiasm, voxels in this region will include several different fiber directions and the diffusivities in such voxels will thus be an average of several fiber orientations. As a consequence, the standard second order tensor model, which assumes one principal diffusion direction per voxel, may be poorly suited for the chiasm, but, on the other hand, well suited for the parallel organization of the optic nerves and tracts.

Regarding the final step in DTI analysis – the extraction of DTI measures – different methods have been proposed and applied. The most common methods in the literature so far are ROI methods where the voxels for analysis are selected either manually, based on preexisting anatomical knowledge, or by tractography. DTI measures can also be extracted and assessed by group-comparison methods, such as voxel-based morphometry (VBM) and tract-based spatial statistics (TBSS) [3,42,90]. Group-comparison methods include a registration of all subjects' scans to a common space. Such registration may perform poorly for structures with certain anatomical properties, for example structures that vary anatomically between subjects, that are relatively small, and that are localized in areas prone to image artifacts. The anterior visual pathways are located in such an area of the brain, where the proximity to bone and air-filled cavities (the sinuses) causes abundant *susceptibility artifacts*. This kind of artifacts arises due to differences in the extent of magnetization of different tissue types, which causes micro-gradients near the boundaries of tissues, reducing the signal intensity of voxels in such areas. The resulting susceptibility artifacts increase with increasing field strength.

Carefully hand-drawn ROIs in original diffusion space have the advantage of adapting to changes between scans, but potentially suffer from subjectivity/user-error. Smith et al (2006) compared inter-scan and inter-subject variability between TBSS, VBM and manual ROIs and found that TBSS resulted in the lowest variance for most structures while manual ROIs had the lowest variance for some structures [90]. However, the study by Smith et al focused on white matter tracts that are relatively large, compared to the

anterior visual pathways. In order to assess the effect of ROI method for DTI-data extraction from the anterior visual pathways four different ROI methods were compared in Study III of this thesis.

1.4.3 Pituitary adenomas and visual impairment

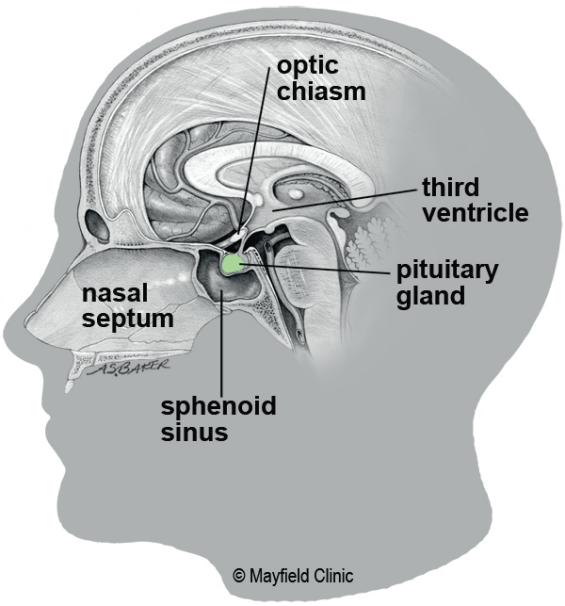

Figure 7. Cross-section of a normal pituitary gland inside the bony sella, with the optic chiasm located just superior. Printed with permission from Mayfield Clinic.

Pituitary adenomas account for 12-15% of symptomatic intracranial neoplasms [116]. While their prevalence in the general population is high – 15% according to autopsy studies and 23% according to radiological studies [36] – only a minority will cause symptoms and require treatment. Small tumors may be silent or cause symptoms caused by an over-production of hormones. Larger tumors (> 10 mm), called macroadenomas, are most often non-productive but may cause visual impairment as they grow and compress the anterior visual pathways, specifically the optic chiasm, located just superior of the pituitary gland (Figure 7). In most cases, the earliest symptom of visual impairment is a visual field deficit [38], where the upper temporal quadrants are affected while the nasal quadrants are relatively spared. This pattern of VFD

is in accordance with the known organization of fibers in the chiasm: the first and major pressure site of the tumors is the central inferior part of the chiasm, where fibers representing the upper lateral quadrants are located. As a tumor grows the VFD will be more extensive, in addition to affected visual acuity and nerve atrophy, eventually leading to complete loss of vision. Macroadenomas may also cause hypopituitarism, by compression of the normal pituitary tissue, and/or compress and affect other adjacent structures, such as the oculomotor and abducens nerves.

Pituitary adenomas

- Benign tumors of the pituitary gland.
- Account for 12-15% of symptomatic intracranial neoplasms.
- Symptoms (most common):
  - Visual deficits, due to compression of the optic chiasm.
  - Underproduction of hormones, due to compression of normal pituitary tissue.
  - Overproduction of hormones.
- Diagnosis by MRI and neuro-ophthalmological examination.
- Treatment by transsphenoidal tumor resection.

Indication for surgery of pituitary macroadenomas

Surgery by transsphenoidal tumor resection is currently the standard treatment for pituitary macroadenomas that affect the visual pathways. It is a well-documented method that is associated with few complications and leads to visual recovery in the majority of cases [46,81,84,95]. Indication for surgery is often 1) an already detected visual impairment or 2) a tumor of a size that is deemed large enough to risk injury to adjacent structures, most often the anterior visual pathways.

Today, the clinical assessment is based on conventional MRI and neuro-ophthalmological examination, including visual field examination. Conventional MRI will determine the size of the tumor and its relation to surrounding structures, but cannot detect functionality and possible microstructural injury of the visual pathways. The neuro-ophthalmological test battery is sensitive to visual impairment, however, the majority of the

tests, including the visual field examination, suffer from subjectivity as the results are based on patient performance. The specific cause of visual impairment may be difficult to determine in the presence of several ophthalmological conditions; for example, visual impairment by a macroadenoma may be difficult to detect and specify in the presence of concurrent glaucoma or macular degeneration. Thus, the current diagnostic tools suffer from subjectivity and a lack of specificity for injury caused by macroadenomas. Furthermore, although most patients will experience visual improvement after surgery, the visual function may not be completely normalized, due to different extents of irreversibility of the injury [59].

Objective diagnostic tools that are sensitive to early injury in the anterior visual pathways would thus be valuable, in order to identify candidates for surgery at an early stage and save visual function. Previous studies have explored methods for objective diagnostics, such as measurements of the suprasellar tumor extension based on conventional MRI and optical coherence tomography (OCT) of the retinal nerve fiber layer (RNFL) [20,27,41,86,106]. The suprasellar tumor extension has been shown to correlate with the level of visual impairment, however, the inter-individual variability seems to be large and the method is thus difficult to rely on in individual cases. Preoperative OCT of the RNFL has been demonstrated to be predictive of the postoperative visual outcome and may thus be considered for objective diagnostics. However, it may not be optimal for diagnostics that aim to identify early signs of injury in the visual pathways, as the RNFL can be normal despite visual field deficits that are measurable with perimetry [27,52].

In Study IV in this thesis we assess the ability of DTI to detect injury in the anterior visual pathways, specifically the optic tracts, in patients with pituitary macroadenomas.

1.4.4 Compression injury at the microstructural level

What is the nature of the microstructural injury in the anterior visual pathways caused by tumor compression? In other words, what kind of injury may DTI be able to detect? Several groups have studied and discussed the specific pathology, either by clinical follow-up studies of patients after tumor resection or by simulated tumor compression and decompression in animal studies. The clinical studies have suggested at least two phases of visual recovery after decompression: 1) an early phase that occurs within days after surgery and 2) a later phase within 1 to 4 months after surgery [48,57]. A proposed explanation for the early recovery phase has been removal of conduction block and/or recovery of the cytoskeleton. The late recovery

phase has been explained by remyelination. These proposed mechanisms of recovery are in accordance with the simulated animal studies where chronic compression of the cat optic nerve has been shown to lead to a gradual demyelination, in combination with partial axotomy [26]. Furthermore, by monitoring nerve conduction after decompression by means of implanted electrodes, an early and a late phase of recovery could be observed [26]. Microscopic analysis revealed a remyelination that followed the time course of the late recovery phase. There was no recovery of the axons that had undergone axotomy.

AIMS

The purpose of Study I and II was to assess the ability of tractography to visualize the optic radiations, with the ultimate goal to reduce visual deficits caused by surgery in the temporal lobes.

Specific aim, Study I: To compare tractographies of Meyer's loop by two different tractography algorithms - deterministic and probabilistic – and to determine which one produces the most anatomically accurate results.

Specific aim, Study II: To compare and validate the accuracy of tractographies of Meyer's loop by two different tractography algorithms – deterministic and probabilistic – by correlating tractography results to postoperative perimetry results, in patients who have undergone temporal lobe resection.

The purpose of Study III and IV was to explore the ability of DTI to assess the anterior visual pathways – specifically the optic tracts – with the ultimate goal to assess DTI as an objective diagnostic tool for injury caused by compression by pituitary adenomas.

Specific aim, Study III: To compare data extraction by different region-of-interest methods in clinical DTI scans of the optic tracts, in order to identify possible differences due to method as well as the most reliable method.

Specific aim, Study IV: To explore whether DTI can be used for objective assessment of the optic tracts, in order to find and grade injury caused by pituitary adenomas that compress the anterior visual pathways.

SUBJECTS AND METHODS

Study design

Study I and III are methodological studies of an exploratory nature. Study II and IV are prospective cohort studies. Power calculations were not possible due to the limited number of eligible patients.

Ethical considerations

The studies of this thesis were approved by the regional ethical board of the University of Gothenburg and performed according to statutes of the Declaration of Helsinki. Informed oral and written consent was obtained from all subjects prior to inclusion in the studies.

All studies included non-invasive MR imaging. In addition, Study III and IV included study-specific neuro-ophthalmological examinations. Both procedures were considered safe for the participants. All MRI scans, of patients and controls, were clinically assessed by a neuroradiologist in order to detect pathological findings.

1.5 Subjects

All subjects were included and assessed at the Sahlgrenska University hospital, Gothenburg, Sweden.

In Study I, DTI was performed on eleven controls (mean age 34 years, range 23-62 years) without neurological or psychiatric disease and in seven patients (mean age 36 years, range 15-58 years) with refractory temporal lobe epilepsy before (five patients) and after temporal lobe resection (seven patients).

For Study II, eight patients with temporal lobe epilepsy who were to undergo TLR were included consecutively between 2007 and 2011 (age range, 15-38 years; median 34; 2 male). All patients had normal visual fields before surgery. Five out of the eight patients were operated within the epilepsy surgery program (also included in Study I). The main indication of surgery for the remaining three patients was tumor resection.

For Study III and IV, 20 controls with normal vision (apart from refractive errors) were included (age range 30-61 years, mean 44; 7 male). In addition, 23 patients with pituitary adenomas, scheduled for transsphenoidal tumor

resection, were included for study IV (age range 28-70 years, mean 52; 14 male). A suprasellar tumor extension of grade 2-4 according to the SIPAP grading system was required [33]. The patients were included consecutively between April 2012 and August 2015.

1.6 Methods

Imaging

For all studies, both DTI and conventional MRI were performed on a Philips 1.5 T scanner with some variations in associated software, hardware and protocol settings (see respective article for more exhaustive descriptions). 1.5 T was selected instead of 3 T in order to decrease image distortion caused by magnetic susceptibility, abundant in both the Meyer's-loop and the optic-chiasm areas. For the DTI acquisition, a single shot spin echo EPI pulse sequence was used. In order to further prevent image distortion by magnetic susceptibility, a relatively high sensitivity encoding (SENSE) factor (3.2) was selected. However, both high SENSE factor and lower magnetic field strength lead to reduction of the signal-to-noise ratio (SNR), why increased signal averaging (NSA) was used as compensation. The number of NSA was three to six, in combination with 15 (study I and II) or 32 diffusion-sensitizing gradient directions (study III and IV) (b = 800 s/mm^2). Reconstructed pixel size was 1.9mm×1.9mm. DTI scan time was approximately 13 to 16 minutes.

DTI-data post-processing

In all studies, FMRIB's Diffusion Toolbox (FDT, part of FSL) was used for motion and eddy current correction, preceding probabilistic tractography or data extraction (http://fsl.fmrib.ox.ac.uk/fsl/fslwiki) [113]. For Study I and II, these corrections were carried out with another software preceding deterministic tractography: the "FiberTrak" package, part of the Extended MR Workspace (EWS) by Philips. For Study III and IV, the voxels of the diffusion images were interpolated to an isotropic size of 1 mm^3, using a sinc-like spline interpolation [51], as the first step of the post-processing.

Tractography

Deterministic tractography was carried out by the FiberTrak package, part of the EWS by Philips. This fiber tracking software is based on the "fiber assignment by continuous tracking" (FACT) algorithm [68,94]. Thresholds for the tractography were: FA > 0.25, maximum angle change = 90 degrees and minimum fiber length = 30 mm. Multiple ROIs were selected to dissect the

optic radiation, as previously described [74]. Following the initial ROIs, the tractography was calculated and visualized. Additional ”trimming” ROIs were then defined in order to exclude apparently spurious fibers. Computation time for diffusion registration, creation of FA maps and tensor calculation was approximately 10 minutes. Computation time for tractography of the optic radiation was 20-30 minutes per side.

Probabilistic tractography was carried out using the BEDPOSTX and the PROBTRACKX tools in FSL (version 5.0.4), which allows modelling of crossing fibers within voxels (i.e. ball and stick) [10]. For Study I and II, the maximum angle between voxels was set to 90 degrees; default angular threshold in FSL is approximately 80 degrees, which was considered too restrictive in the case of Meyer’s loop, due to its known curving course.

For Study I and II, tractographies, including ROI definition, and TP-ML measures were carried out by two independent operators and repeated once by one operator, for calculations of inter- and intra-rater agreement. TP-ML was measured in axial slices, as the distance between the temporal pole and the most anterior limit of the Meyer’s-loop tractography (Study I and II) (Figure 6). The postoperative resection length was measured as the distance between the former temporal pole and the posterior border of the resection (Study II).

Region-of-interest methods

In Study III, four ROI methods were applied for DTI-data extraction from the optic tracts: manual tracing was performed in 1) the b0 image and 2) a T1-weighted image registered to the FA image and semi-automatic segmentation was performed based on 3) tractography and 4) the FA-skeleton algorithm in the tract-based spatial statistics framework (TBSS) [90]. For the latter method, the skeleton algorithm was applied on each FA map, keeping the original space of each individual FA map. Voxels with FA<0.2 were excluded in order to exclude voxels with primarily gray matter or CSF. Voxel selection was restricted to voxels included in the FA skeleton that represented the OT. This FA-skeleton method was also used for data extraction in Study IV.

Visual field examination

For Study II, all patients underwent pre- and postoperative visual field examination by Goldmann perimetry, part of the local clinical protocol for TLR. The results were analyzed by two experienced senior neuro-ophthalmologists and categorized as: no VFD (VFD=0), VFD smaller than one quadrant (VFD<q), and VFD equal to one quadrant (VFD=q).

For Study III and IV, patients and controls underwent visual field examinations by HR perimetry, performed by an experienced perimetrist. HR perimetry was selected for three reasons: 1) the method yields numerical results making it more easily quantifiable, 2) there was a robust local experience and 3) it has been shown to reveal chiasmal syndrome with a sensitivity at least equal to more generally used methods [22,39].

Statistical analysis

Descriptive statistics was used for comparisons to dissection studies in Study I and II. In Study III, the distribution of data was described by mean, standard deviation (SD) and coefficient of variation (CV) of FA for each ROI method.

For **comparisons of differences between groups**, Fisher's non-parametric permutation test for matched pairs was used in Study II. For comparison of differences between more than two groups, covariance pattern models and mixed models were used, in order to account for dependencies within individuals (Study I, III and IV). Adjustments for multiple comparisons were made by the Tukey-Kramer method.

For analysis of **correlation** between two variables, Spearman's rank correlation coefficient was used in Study II. Pearson's correlation coefficient was used in Study IV and, due to testing of several correlations on related variables, a summarizing ANOVA-test was also conducted using a mixed model. Correction for multiple testing was made by interpreting the individual test as significant only if the corresponding summarizing test was significant.

Inter- and **intra-rater reliability** was analyzed using Intraclass Correlation Coefficient (Study I and II). Repeatability coefficients and limits of agreement were used for the same purpose in Study III. Jaccard analysis was used to test the level of overlapping voxels between the methods in Study III.

For Study IV, a **prediction model** based on logistic regression, with twelve possible predictors, was constructed. Forward selection with Akaike's information criterion (AIC) was used in order to find the combination of predictors with the best discriminative ability. Leave-one-out cross-validation was performed to validate and compare models. The best model was selected based on the cross-validation results, statistical significance of included predictors as well as the lack of strong correlations between included predictors

Statisticians from Statistiska konsultgruppen, Gothenburg, were consulted for all studies of the thesis.

RESULTS

1.7 Study I

For controls and patients together, there were statistically significant differences ($p<0.01$) for TP-ML between all methods thresholded at PTG ≤1% compared to all methods thresholded at PTG ≥5% and DTG. There were no statistically significant differences between PTG 0.2%, 0.5% and 1% or between PTG 5%, 10% and DTG. For the controls and patients separately the results were similar, except for one comparison: in the patient group there was no significant difference between PTG 1% and DTG ($p = 0.07$).

The inter- and intra-rater variability tests, based on TP-ML measures of the 23 scans, showed good to excellent agreement (ICC 0.6-0.8 inter-rater, ICC 0.7-0.9 intra-rater) [37].

TP-ML measures of the eleven controls revealed a closer match to dissection studies for PTG ≤ 1% than PTG ≥ 5% and DTG.

1.8 Study II

Post-operative perimetries were analyzed and degrees of VFD were determined. Three patients had no VFD, two patients had a VFD of less than one quadrant and three patients had a VFD equal to one quadrant.

The difference between preoperative TP-ML (by DTG and PTG separately) and resection length could predict degree of postoperative VFD (DTG: r_s=-0.86, $p<0.05$; PTG: r_s=-0.76, $p<0.05$). Resection length alone could also predict the degree of postoperative VFD (r_s=0.73, $p<0.05$). Neither preoperative TP-ML nor the difference between pre- and postoperative TP-ML could predict postoperative VFD.

The difference between DTG- and PTG-determined median TP-ML was 6 to 8 mm. Median pre-operative TP-ML distances for the non-operated sides were 42 and 35 mm, as determined by DTG and PTG respectively and results by PTG were thus a closer match to dissection studies (Table 1).

ICC for inter-rater reliability was 0.4 for DTG and 0.7 for PTG.

1.9 Study III

The resulting FA values divided the ROI methods into two groups that differed significantly: 1) the FA-skeleton and the b0 methods showed higher FA values compared to 2) the tractography and the T1-weighted methods. The latter relationship was true for all sections but section 1 (the most anterior 5 mm) where the tractography and the manual T1W methods also differed significantly.

The mean difference between measurements from the two raters (inter-rater) was found to be close to zero for all methods and positions. The intra- and inter-rater variabilities were similar for all methods, except for the tractography method where the inter-rater variability was higher. The inter-scan variability was found to be slightly higher than the inter- and intra-rater variabilities for all methods. The FA-skeleton method had a better overall reproducibility than the other methods.

When comparing ROI methods the Jaccard indices were in general low (~0.3). The highest Jaccard index between methods was found between the FA-skeleton and the manual b0 method.

1.10 Study IV

Eleven out of the 23 patients had pathological visual fields before surgery. All patients with VFD improved after surgery, although four patients had remaining VFD at the evaluation six month after surgery. Three patients showed clinical signs of optic nerve atrophy, which remained unchanged after surgery.

None of the statistical analyses lead to significant results when DTI measures from the most anterior ROI (ROI 1) were included; the paragraphs below regard results from ROI 2 and 3.

Both the degree of VFD and chiasmal lift were significantly correlated with the radial diffusivity **(**$r = 0.55$, $p < 0.05$ and $r = 0.48$, $p < 0.05$, respectively**)** and the fractional anisotropy (FA) ($r = -0.58$, $p < 0.05$ and $r = -0.47$: $p < 0.05$, respectively). There were no correlations with axial diffusivity, for neither VFD nor chiasmal lift.

The axial diffusivity differed significantly between controls and patients with VFD, both before and after surgery ($p < 0.05$), however no significant differences were found between patients with and without VFD nor between

controls and patients without VFD. There were significant differences in FA between controls and patients with VFD before surgery (ROIs 2 and 3), but only a trend towards such a difference after surgery ($p = 0.058$, ROI 3). Before surgery, the patients with VFD had lower FA than all other groups, although this difference was only significant compared to the controls. Before surgery there was a trend towards higher radial diffusivity in the patient group with VFD compared to the controls ($p = 0.073$, ROI 3).

The selected prediction model was based on axial diffusivity from ROI 2 and 3 and FA from ROI 3. The model classified all patients with VFD correctly (sensitivity = 1), whereas 17 out of 20 controls were classified as controls (specificity = 0.85). Nine out of twelve patients without VFD were classified as patients (sensitivity = 0.75) (Figure 9).

DISCUSSION

1.11 Discussion – Study I and II

Study I and II both aimed to validate the anatomical accuracy of tractography of Meyer's loop. Study I did so by comparison to results of dissection studies and Study II, by prediction of postoperative visual outcome based on preoperative tractography. In addition, the studies included two commonly used tractogrpahy algorithms – DTG and PTG – with the aim to reveal possible differences in their delineation of Meyer's loop.

Meyer's loop could successfully be visualized by tractography in all subjects in both studies – controls and patients, by DTG and by PTG. The anterior extent differed significantly between the algorithms: PTG placed Meyer's loop almost 1 cm more anteriorly than DTG. Furthermore, PTG was the closest match to dissection studies, although results by PTG systematically placed Meyer's loop more posteriorly than dissection studies. PTG proved to be the more robust algorithm with respect to reproducibility. Despite significant differences between the algorithms, both DTG and PTG could predict the degree of postoperative VFD based on preoperative tractography.

1.11.1 The tractography algorithm and Meyer's loop

Several factors may affect the end result of tractography delineation, from the scanning procedure and MRI protocol to the variables of the tractography generation, including selected tractography algorithm [55]. Awareness of these factors and their effects is crucial in the interpretation and comparison of tractography studies, and indeed for the clinical application.

As revealed by Table 1, the TP-ML results of Study I and II are similar to other tractography studies of Meyer's loop, including the differences between DTG and PTG, where results by PTG are closer to those of dissection studies. This may be explained by an ability of PTG to better cope with the crossing and kissing fibers in the Meyer's-loop region than deterministic models, as PTG allows for an uncertainty of diffusion orientation which makes it less likely to exclude voxels with low FA and interrupt tracking at such voxels [54,117]. As Meyer's loop has a curving shape and the optic radiation is adjacent to several other white matter tracts, DTG may be suboptimal for tractography in this region.

Table 1. The anterior extent of Meyer's loop – results as reported from cadaver dissection and tractography studies.

Author/Year	**Study population**	**Method**	**TP-ML (mm):** mean (range)
Peuskens et al. 2004[82]	17 controls	Cadaver dissection	27 (15-30)
Ebeling and Reulen 1988[32]	25 controls	Cadaver dissection	27 (22-37)
Chowdhury and Khan 2010[24]	11 hemispheres	Cadaver dissection	26 (23-31)
Rubino et al. 2005[85]	20 controls	Cadaver dissection	25 (22-30)
Yamamoto et al. 2005[115]	5 controls	DTG	37 (33-40)
Nilsson et al. 2007[74]	7 controls 2 patients	DTG	44 (34-51): controls 46 (40-51): patients
Taoka et al. 2008[97]	14 patients	DTG	37 (30-43)
Chen et al. 2009[23]	48 patients	DTG	32 (21-51)
Dreessen de Gervai et al. 2014[30]	20 controls	DTG	43 (28-54)
Sherbondy et al. 2008[89]	8 controls	PTG	28 (25-31)
Yogarajah et al. 2009[117]	21 controls 20 patients	PTG	35 (24-47): controls 34 (24-43): patients
James et al. 2015[49]	75 controls	PTG	37.44 (32.2-46.6): left 39.08 (34.3-49.7): right
Anastasopoulos et al. 2014[1]	10 patients	DTG PTG	41 (39-43): DTG, depicted in 3/10 patients 34 (23-40): PTG, depicted in 9/10 patients
Lilja et al. 2014[61]	11 controls	DTG PTG	44 (34-51): DTG 33 (25-48): PTG
Borius et al. 2014[16]	13 controls 18 patients	DTG PTG	26: DTG 30: PTG
Lim et al. 2015[62]	20 controls	PTG CSD	35 (23-45): PTG 30 (20-34): CSD

DTG = Deterministic tractography; PTG = Probabilistic tractography; CSD = Constrained spherical deconvolution

The region-of-interest (ROI) selection for tractography may also affect the end result. The ROIs define the start and end points, and sometimes also waypoints and exclusion points, for tractography. Study II found a lower inter-rater reproducibility for DTG than for PTG. In the DTG process several additional "trimming" ROIs have to be added to the standardized ones in order to exclude aberrant fibers – a step that is not required in the PTG process. The additional ROIs for DTG are selected by the operator, differently in each individual scan, resulting in several operator- and scan-specific ROIs. Subjectivity thus becomes a major issue for DTG of Meyer's loop, and could explain the lower reproducibility (Figure 8).

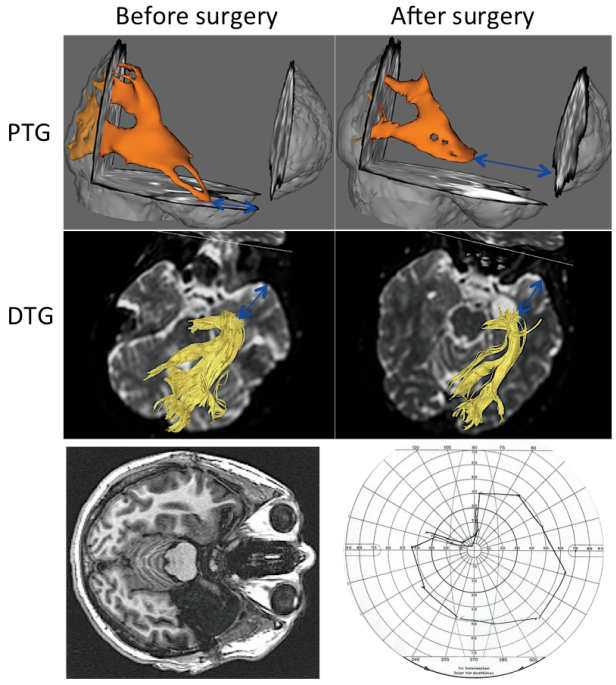

Figure 8. Case example of a patient who suffered a visual field defect after TLR. Tractography by PTG showed a significant increase of TP-ML after surgery, consistent with the visual defect, while no such change could be seen using DTG in this case.
Upper row: PTG before (left) and after (right) TLR. Middle row: DTG before (left) and after (right) TLR. Blue arrows indicate the distance between the temporal pole and the anterior limit of Meyer's loop (TP-ML). Lower row: Post-operative T1 (left) and perimetry (right).

In the majority of tractography studies of Meyer's loop, the ROIs are manually drawn based on the operators' prior anatomical knowledge. Attempts to automate this step have been made but have not yet proven to be as successful as the manual method [112]. The reason may be important individual anatomical differences as well as anatomical distortions in brains with pathology, which automated methods cannot adjust to.

Similar to Study I and II, other studies have compared DTG and PTG from the same data set [1,16]. Anastasopoulos et al. (2014) arrived at similar TP-ML measures as the studies in this thesis, however, the DTG measurements were based on few subjects (n=3) as DTG failed to depict Meyer's loop in most subjects in their group. Borius et al. (2014), on the other hand, arrived at TP-ML measurements of the opposite relation as Study I and II: DTG placed Meyer's loop more anteriorly than PTG. However, the threshold for maximum angle between principal diffusion directions of two tracking steps for PTG was unusually small in the latter study – approximately 37 degrees – whereas most studies use an angle of around 90 degrees. Similarly, James et al (2015) used PTG and a maximum angle of 30 degrees, in 75 controls, and arrived at longer TP-ML measures than most equivalent PTG studies (Table 1) [49].Thus, the angle threshold most likely has a significant effect on the tracking in the sharply bending region of Meyer's loop.

The implication of the angle threshold highlights the importance of threshold settings and possible effects on tractography of Meyer's loop. The effect of the FA threshold (used to determine below which FA value tracking should be stopped) has been discussed and assessed. Chen et al. explored the location of Meyer's loop using DTG with an FA threshold of 0.15; such a low FA threshold could increase the sensitivity of finding the most anterior fibers in a region where partial volume effects will occur [23]. Indeed, the resulting TP-ML measures were as close to dissection studies as most PTG studies. Thus, it could be argued that the deterministic technique could produce similar results as the probabilistic one if performed by experts in white matter anatomy (for an adequate trimming procedure) and using low enough FA-threshold settings.

1.11.2 Validation of tractography

Validation of the anatomical accuracy of human *in vivo* tractography is a challenge as there is no "ground truth" for comparison. Nevertheless, several methods have been proposed and assessed.

Dissection studies based on Klingler's fiber dissection technique[63] have often been used as a gold standard. Such comparisons in Study I and II showed that PTG was a closer match to dissection results, although TP-ML by PTG was systematically longer (i.e. Meyer's loop more posteriorly located) than the measures of dissection studies (Table 1). However, this does not necessarily mean that the probabilistic algorithm is insufficient, as the accuracy of dissection results have been questioned. A certain deformation level has been seen to occur during the dissection, possibly due to the extraction of the brain from the cranium, shrinking of the tissue during fixation by formalin and fissuring of the tissue due to freezing. The deformation level has been shown to vary between different brain structures and regions but the specific deformation of the Meyer's-loop region is unknown. However, global brain volume shrinkage of 8.1% has been reported[87] and the TP-ML measures from dissection studies may thus be artificially shorter than those of a living brain, which should be taken into account when evaluating the systematic difference seen in comparison to tractography.

Other methods for validation have been suggested, such as MRI-detectable neuronal tracers in animal studies, where a tracer, such as manganese, is injected into a tract of interest. Dyrby et al. compared results from manganese-enhanced imaging to probabilistic tractography, and concluded that the latter reliably detected specific pathways, including the optic radiation [31]. To ensure the absence of most of the sources known to degrade the accuracy of *in vivo* DTI tractography, they performed their experiments on *post mortem* porcine brains. Although these results are promising for the validation of tractography, the accuracy of tractography in *in vivo* human brains still remains to be determined.

A few groups have attempted *in vivo* validation of tractography by prediction of postoperative visual outcome in patients who undergo TLR, using either DTG or PTG [23,74,83,97,110,117]. The prediction models have all been successful, however, to different degrees. Several of the studies have been able to predict postoperative VFD when combining tractography and resection length measurements, similar to Study II herein. Taoka et al., using DTG in a study of 14 TLR patients, found that preoperative TP-ML and resection length together could divide their cohort into two groups: those with no or small visual field defects and those with larger visual field defects [97]. In a PTG study based on 20 TLR patients, Winston et al. found similar correlations and were able to predict degree of postoperative visual field defect, comparing resection length and preoperative TP-ML [110].

These prediction studies provide a certain confirmation of the anatomical accuracy of tractography in live human brains. However, a variety of tractography methodologies are represented in the prediction studies, including different tractography algorithms. As there are known differences in the ability of different tractography algorithms to depict the anterior extent of Meyer's loop, one could assume that these studies validate the accuracy of tractography with a certain margin of error. This assumption is reinforced by the results of Study II, where the degree of postoperative VFD can be predicted using both DTG and PTG.

1.11.3 Tractography during temporal lobe resection

Although validation of the anatomical accuracy of tractography is of interest, the ultimate goal of tractography of Meyer's loop for TLR is not a perfect delineation but rather a method that can reduce postoperative visual deficits. Thus, as yet another means of validation, tractography may be integrated in the TLR process and the frequency and degree of postoperative VFD may be assessed.

To this date, two scientific articles have reported results of pre- and intraoperative tractography during TLR and the effect on postoperative visual outcome. Thudium et al. (2010) applied preoperative tractography in a surgical neuronavigation system in 12 patients, attempting to plan safe surgical trajectories of resection to avoid injury to Meyer's loop [100]. There was no control group in this study, however, 75% of the patients had no postoperative VFD, compared to 53% in a previous study from the same group. Winston et al. (2014) displayed preoperative tractography on a neuronavigation system intraoperatively as well as in the operation microscope [111]. None of their 21 patients had a postoperative VFD large enough to preclude driving, which was the case for 13% of the patients in a previous cohort of 44 patients. They concluded that intraoperative tractography guidance for the surgeon reduces severity of visual outcome, while preserving level of seizure outcome. Further randomized prospective studies with control groups, and larger cohorts, are needed to confirm these findings.

1.11.4 Improving tractography algorithms

Modeling the diffusion distribution in each voxel as a 3x3 symmetric tensor, as for DTG, is the most common approach in clinical DTI practice today. However, it seems this modeling is not able to resolve complex intra-voxel

microstructures (e.g. crossing fibers), which are deemed to exist in at least one third of all white matter [10]. In order to address this problem a wide variety of multi-fiber diffusion models have been proposed, including the 'ball and stick' model used for PTG herein [11], analytical q-ball imaging [29] and non-negativity constrained spherical deconvolution (CSD) [102]. A comparison of different multi-fiber models, in terms of false-positive and false-negative fiber detection rates, reported that the "ball and stick" and the CSD models were superior for most tracts, and that the CSD model was superior when it came to voxels including more than two fiber directions [109]. CSD has also been shown to successfully visualize the optic radiation including Meyer's loop [101].

Similarly, two studies compared the sensitivity and specificity of different tractography models, by comparison to results of manganese tracing in animals [58,99]. They both found that a model will either yield high sensitivity and low specificity or *vice versa*, especially in regions of crossing fibers. Thomas et al (2014) concluded that diffusion tensor tractography has fundamental limitations when it comes to accurately mapping brain connectivity and that those limitations are unlikely to be overcome by improvements in data acquisition and analysis. While this judgment may be true when it comes to accurately mapping the human connectome, tractography may still be highly useful clinically. Based on the knowledge of the limitation of different models, specific tractography models may be selected for specific clinical needs. For example, if the objective is to reduce the risk of including false-positive pathways, a stricter model such as DTG or probabilistic ball and stick model with conservative thresholds may be used. On the other hand, if it is important not to miss any pathways of a tract, for example in order to safely prevent surgical injury, a model with higher sensitivity may be used, such as CSD or ball and stick with liberal thresholdings.

1.12 Discussion – Study III and IV

1.12.1 Choice of ROI method matters (Study III)

Choice of ROI method for DTI-data extraction was found to significantly affect the FA values when the OTs were analyzed. The results of Study III highlight the importance of carefully considering the methodology of DTI analysis, for small structures of interest in particular. The optimal methodology may differ depending on the specific qualities of a structure of

interest, including its dimensions, the fiber organization, the location and surrounding structures, etc.

For the analysis of the OTs there are several structure-specific qualities to consider.

First, the OTs are small in comparison to standard DTI voxel dimensions. An appropriate ROI method should thus be able to accurately identify the OTs, while avoiding border-zone voxels and voxels that are outside of the tracts, as inclusion of such voxels would have a significant influence on the resulting mean diffusivities. Tractography may be used for ROI definition; however, in Study III, tractography performed poorly for analysis of the OTs, mainly due to inclusion of non-optic tract and border-zone voxels.

Second, the OTs are located in an area prone to image distortion due to magnetic susceptibility artifacts, affecting the image quality and geometry. ROI methods based on registration between diffusion space and other images, such as T1-weighted and/or standard-space images, may thus result in insufficient overlap of voxels. This was the case for the ROI method that involved registration between T1-weighed images and diffusion space in Study III; the result was spuriously low FA values, similar to those of the tractography ROIs. The registered images were off by one or two voxels at several locations along the OTs, which proved sufficient to significantly affect the results.

Third, for analysis of voxels of the optic chiasm, the crossing of fibers within voxels should be considered, as DTI measures from a single voxel will be an average of several fiber directions. In Study III, the results from ROI 1, which included chiasmal voxels, differed from results from the more posterior ROIs, which included only OT voxels.

The ROI method based on the FA-skeleton algorithm of TBSS performed the best [90], defined as a comparatively high anatomical accuracy and reproducibility. Standard TBSS includes a registration step, which was deliberately excluded for the ROI method herein due to the expected difficulties of registration discussed above. The manually drawn ROIs performed similarly to the FA-skeleton method, however, the reproducibility was slightly poorer, most likely due to the difficulty for the human eye to accurately identify all sections of the small OTs. In contrast to the subjectivity of the manually drawn ROIs, the FA-skeleton method is semi-automatic, as the algorithm selects the voxels to be included, and thus less sensitive to user error.

While the ROI method based on the FA-skeleton performed well for the OTs, this may not be the case for other structures. The FA-skeleton normally defines two voxels per cross section, which is similar to the dimensions of the OT without including border-zone voxels. A larger tract will have a wider center, where some of the voxels may be affected by pathology with decreased FA and some not. In such a case, the FA-skeleton ROI method would miss the pathologically affected voxels by centering on the ones with the highest FA.

In conclusion, several structure-specific qualities will affect the suitability of a ROI method. The method proposed herein may be considered for structures with similar qualities as the OTs.

1.12.2 DTI as a diagnostic tool (Study IV)

The results of study IV demonstrated that DTI can detect pathology and degree of injury in the anterior visual pathways, affected by compression by pituitary adenomas. These findings are promising in the quest for an objective diagnostic tool that can assist in the treatment-decision process for patients with pituitary adenomas. The specific variations of diffusivities that were detected may reflect specific pathologies: the positive correlation of radial diffusivity and degree of VFD may stand for a gradual demyelination concurrent with a worsening visual function and the low level of axial diffusivity in the patient group may stand for a degree of axonal atrophy in the OTs that are affected by external pressure.

A prediction model could successively separate patients from controls, based on a combination of DTI measures (Figure 9). The model was primarily based on axial diffusivity and, secondarily, on FA. According to the animal-model studies referred to in Section 1.2.2, a decrease in axial diffusivity may be a marker for axonal degeneration. The prediction model could thus reflect considerable differences in the level of axonal degeneration between the groups, in combination with more unspecific conditions affecting the anisotropy (i.e. the FA values). A certain level of axonal degeneration is likely in the group of patients with VFD, which could explain why the model classified all patients with VFD as patients. Local, less extensive axonal degeneration, in combination with demyelination, may be present in the group of patients without VFD, which may explain that nine out of the twelve patients without VFD could be classified as patients. A prediction model such as the one presented in Study IV may be used in the preoperative assessment of injury to the anterior visual pathways and contribute in the treatment-

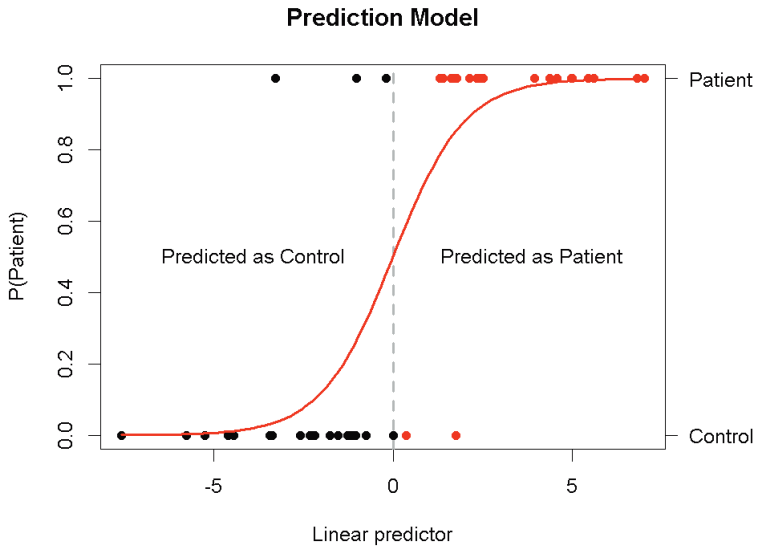

*Figure 9. Prediction model based on three predictors: axial diffusivity (AD) from ROI 2 and 3, FA from ROI 3. Linear predictor: 50 -16*AD_{ROI3} - 22*FA_{ROI3} -6.1*AD_{ROI2} (AD in units of μm^2/ms). ROC AUC (95% CI): 0.91 (0.81; 1).*

decision process. The current model should be tested on a larger cohort in order to be confirmed and/or modified.

Paul et al (2014) analyzed DTI measures in the OTs in a study including nine patients with compressive pituitary adenomas and, similar to Study IV, were able to find significant results based on DTI measures [80]. While both studies resulted in positive correlations between radial diffusivity and degree of visual impairment, they differed in some aspect. In contrast to Study IV, Paul et al. (2014) reported significant differences in radial diffusivity, and no differences in axial diffusivity between patients and controls and, furthermore, they also reported a normalization of radial diffusivity after surgery for the compressive tumor patients. These inconsistencies between the two studies may be due to differences in statistical methods and the fact that both studies were based on relatively few patients, who may differ in level and type of OT injury.

Although the group comparisons in Study IV revealed no significant differences in radial diffusivity between any of the groups, a trend could be observed between controls and patients with VFD before surgery. This trend

disappeared after surgery, along with significant differences in FA before surgery between the same two groups. The difference in FA before surgery may be the result of a combination of affected axial and radial diffusivity. The changes in radial diffusivity and FA after decompressive surgery may be due to a remyelination and thus a normalization of the radial diffusivity postoperatively, however, larger study samples are needed to confirm this hypothesis.

Similarly, there were no significant differences in DTI measures for the patient group with preoperative VFD before compared to after decompressive surgery, although all patients improved postoperatively with regard to visual field. However, although not statistically significant, some differences could be seen: after surgery radial diffusivity was lower and FA higher while there was almost no change in axial diffusivity. Due to a limited study power, these results can neither confirm nor renounce a postoperative difference for patients with preoperative VFD.

The FA-skeleton ROI method, which was the most successful in the methodological Study III, was applied in study IV, including the definition of three separate ROIs covering the anterior portion of the OTs in an anterior-posterior direction. The purpose of the three ROIs at different distances from the optic chiasm was to explore the possibility of varying microstructural changes, and thus diffusivities, along the OTs. Such variations could be expected, based on the results of Study III and the study by Paul et al (2014), which both revealed a pattern of varying DTI-measure values along the length of the OTs: for example, lower FA close to the chiasm and an increase in FA more posteriorly [80]. Furthermore, ROI 1 (closest to the chiasm) was expected to differ from the other ROIs due to inclusion of chiasmal voxels, which would affect the DTI measures due to crossing fibers. The more anterior ROIs would also be directly affected and flattened by tumor compression. The results of Study IV revealed that the different ROIs indeed provided unique information as, for example, AD from both section 2 and 3 were selected for inclusion in the prediction model. In the group comparisons no differences could be seen for ROI 1 and ROI 1 did not contribute to the prediction model. Thus, the optimal ROI location for assessment of injury due to external chiasmal compression may be one or several ROIs across the anterior sections of the OTs, while excluding the chiasm.

1.13 Strengths and limitations

The MRI protocol that was used for DTI acquisition in all four studies may be discussed in this section, as it may be argued to imply strengths, primarily, but also limitations. The Meyer's-loop and the OT areas both risk image distortion due to susceptibility artifacts and, furthermore, the common aim of the studies was to depict relatively small structures with precision, especially in the OT region. The magnetic field strength in combination with the protocol settings were selected in order to optimize imaging for these conditions.

The DTI acquisition may have limitations. More recent techniques for reduction of image distortions and increased resolution, such as zoomed acquisitions, were not available at the time of the scanning but may be an option for the small structures that are the anterior visual pathways. Other groups have presented probabilistic tractography results of Meyer's loop equivalent to those of Study I and II, although data has been acquired on 3 T scanners [62,117]. Higher field strength has advantages such as higher SNR and shorter scan times and may be preferable if image distortion factors can be suppressed.

1.13.1 Study I and II

A major strength of Study I and II was the comparison of DTG and PTG based on the same set of DTI scans. While differences between the two algorithms could be observed by comparison of results from different studies, several other differing factors between those studies may have affected the end tractography results, why such comparisons are insufficient.

A limitation of Study I and II was that, although the goal was to compare tractography algorithms alone, some other factors in the comparisons did indeed vary: software, ROI selection procedure and number of tensors per voxel (DTG used a one-tensor model and PTG allowed crossing fibers within voxels). However, the comparisons can be described as clinically relevant since the specific implementations of DTG and PTG in Study I and II are commonly seen in clinical practice and studies.

The reproducibility tests in Study I and II strengthen the credibility of the study results, as certain subjective steps are present in the tractography procedure (eg. ROI definition). Furthermore, the reproducibility of PTG was stronger than that of DTG, which contributes important information about differences between the algorithms.

In Study I, results of both controls and patients were analyzed together. Although the aim of the study was to compare methods rather than to achieve normal anatomy, this lead to a reduction of the homogeneity within the study group.

In Study II, a clinical grading system based on Goldmann perimetry with three categories of VFD was used. Other studies have used more categories, for example by including calculated percentages of visual field loss [110]. Study-specific perimetry and a more detailed visual field scale could have revealed more details in the results.

1.13.2 Study III and IV

The main strength of Study III was the methodological comparison based on the same set of DTI scans. As argued for Study I and II, many factors affect the end results of DTI imaging; methodological studies, changing one parameter at a time, are important to further the understanding and usefulness of DTI.

The focus of Study III may be considered to be narrow as it was limited to the OTs alone. However, the results are likely to be generalizable to white matter pathways similar to the OTs, especially regarding size, although not to pathways with considerably wider cross sections.

The main strength of study IV is the prospective design including an adequate time span between decompressive surgery and follow-up, sufficient for most visual recovery to occur.

Study III and IV both use the same ROI methodology where the most anterior ROI covers a section of the optic chiasm. Due to the fiber organization of the chiasm the second order tensor model that was used may be poorly suited for chiasmal voxels (discussed in section 1.4.2, paragraph 2). DTI of the optic chiasm requires a considerably higher resolution and/or a more advanced tensor model. However, the second order tensor model is well suited for the parallel organization of the OTs and thus for the more posterior ROIs of the studies.

A limitation of study IV was the small study group, which became apparent when the group was divided into subgroups of patients; some important differences between the groups may be lost due to lack of statistical power.

CONCLUSION

- Preoperative tractography by both the deterministic and probabilistic algorithms could predict the degree of postoperative visual field defects in patients who underwent TLR. Due to significant differences in the visualizations of the anterior extents of Meyer's loop by the two algorithms, it can be concluded that the prediction model provides a validation of the anatomical accuracy, although with a certain margin of error.

- Delineation of Meyer's loop by probabilistic tractography was the closest match to data from dissection studies and the most robust in terms of inter-rater reproducibility. Probabilistic tractography may be recommended for visualization of Meyer's loop, preceding temporal lobe resection, with the goal to avoid injury that leads to postoperative visual deficits.

- Choice of ROI method for DTI-data extraction from the optic tracts significantly affected the resulting DTI measures. A semi-automated method based on the FA skeleton proved to perform the best, in terms of anatomical accuracy and repeatability. The choice of methodology for DTI-data extraction of relatively small white matter pathways should be carefully considered.

- DTI data revealed pathological changes as well as degree of injury in the anterior visual pathways, affected by compression by pituitary adenomas. DTI may provide objective data, detect early signs of injury and become an additional diagnostic tool for determining indication for surgery in the case of pituitary adenomas.

FUTURE PERSPECTIVES

Recent studies have shown that tractography algorithms such as the probabilistic ball and stick model or CSD may be suitable choices for tractography of Meyer's loop as they produce the best matches to known anatomy. The downside of both models, however, is the risk of producing a false positive pathway extent. Even so, with the goal to depict Meyer's loop in order to avoid injury during surgery, these models may be preferred to others that are likely to produce false negative results; a false positive pathway extent may be considered a safety margin. Either way, the surgeon's knowledge of white matter anatomy and awareness of the sources of error of the selected tractography technique is crucial for optimal and safe clinical employment.

Further methodological studies may improve tractography of Meyer's loop, however, studies that evaluate the ultimate goal – reduction of postoperative visual deficits – may be more clinically relevant at this stage. While promising results recently have been published (Winston et al., 2014)[111], these results need to be reproduced based on larger cohorts and, preferably, at different study sites.

Future improvements of the DTI protocol may yield higher resolution and reduction of image distortion of clinical scans. Such improvements would facilitate DTI analysis of small structures especially, such as the anterior visual pathways. Zoomed acquisitions may be such a technique, provided it is realistic to perform in clinical settings.

To this date, there is no consensus about the DTI acquisition procedure, from scanner to data analysis, although several methodological factors clearly affect the end results. More knowledge about methodological effects is needed in order to further introduce DTI as a clinical tool, including for the definition of reference intervals.

Study IV presented promising results about DTI as a possible objective diagnostic tool for injury of the anterior visual pathways in patients with pituitary adenomas. The predictive model based on a combination of DTI measures should be repeated, confirmed and possibly modified based on a larger patient cohort. Possibly, other objective indices such as OCT or tumor extension may be added to the model in order to reinforce its predictive value.

SAMMANFATTNING PÅ SVENSKA

Synbanorna i hjärnan består av nervceller som leder information från ögats näthinnor till primära syncentrum i bakre delen av storhjärnan. En skada på synbanan leder ofta till ett synfältsbortfall, som är specifikt för den del av banan som skadats. Synfältsbortfall är handikappande för individen i olika grad och kan till exempel leda till körkortsförbud.

Diffusion tensor imaging (DTI) är i dagsläget den enda teknik som kan avbilda nervbanor i hjärnan, inklusive synbanan. DTI mäter vattenmolekylers diffusionsrörelse, vilken begränsas och riktas beroende på omkringliggande strukturer, såsom nervernas cellmembran. Nervbanors anatomi och eventuella skadegrad kan på så vis beräknas och avbildas – så kallad *traktografi*. Olika diffusionsegenskaper kan dessutom korreleras till olika typer av skada, såsom nedbrytning av nervceller eller förlust av det isolerande fettlagret runtom nervtrådar (*demyelinisering*).

Operation i tinningloben (*temporallobsresektion*) kan vara indicerat för att avlägsna vävnad som innehåller tumör eller ärrbildning som utlöser epileptiska anfall (*temporallobsepilepsi*). En del av synbanan - *synstrålningen* - passerar genom tinningloben och kan lätt skadas vid temporallobsresektion och leda till förlust av ¼ av synfältet.

Studie I och II syftar till att undersöka om traktografi kan avbilda synstrålningen i temporalloberna korrekt, så att denna bildinformation kan användas inför och under operation för att undvika kirurgisk skada. I studie I jämfördes resultaten av två olika traktografialgoritmer – *deterministisk* och *probabilistisk*. Avbildning med probabilistisk traktografi placerade synstrålningen längre fram, vilket stämde bättre överens med resultat från dissektionsstudier. Studie II baserades på traktografi och synfältsmätningar av åtta patienter som genomgått temporallobsresektion. Uppskattad skadegrad av synstrålningen efter operation, baserat på traktografi, korrelerade väl till grad av synfältsskada. Sammanfattningsvis visar studie I och II att traktografi – särskilt den probabilistika varianten – kan avbilda synstrålningen med en acceptabel anatomisk felmarginal och därmed vara användbar för temporallobsresektion.

Hypofystumörer är oftast godartade men kan leda till uttalade synstörningar när de tillväxer och trycker på den ovanliggande synnervskorsningen, som är en del av främre synbanan. Den gängse behandlingen är kirurgiskt avlägsnande av tumören vilket i de flesta fall förbättrar synen utan allvarliga

komplikationer. Idag används synundersökning inkluderande synfältsundersökning och konventionell bildteknik för diagnos och behandlingsunderlag. Synundersökning är dock beroende av patientens medverkan och innebär en subjektiv bedömning av synpåverkan. Det finns idag ingen objektiv metod för att mäta och kvantifiera skada i främre synbanan.

I studie III jämfördes fyra olika metoder att extrahera data från DTI-bilder av främre synbanan, med syftet att identifiera en stabil metod. Mätningar utfördes på 20 friska individer. Resultaten skiljde sig signifikant mellan metoder och en metod utmärkte sig avseende anatomisk överensstämmelse och reproducerbarhet. I studie IV inkluderades 23 patienter som skulle genomgå kirurgiskt avlägsnande av synbanekomprimerande hypofystumörer. DTI och synfältsmätning utfördes före och efter operation. DTI-data extraherades från främre synbanan med hjälp av metoden som framtagits i studie III. Resultaten visade att grad av synfältsnedsättning korrelerade till DTI-värden och att DTI-värden skiljde sig mellan patienter och friska individer. De skillnader som kunde ses i de specifika diffusionsegenskaperna tyder på att DTI kan identifiera demyelinisering och cellnedbrytning samt att DTI kan detektera skada tidigare än konventionella metoder. DTI skulle i framtiden kunna användas för objektiv diagnostik av främre synbanan, vid misstänkt skada orsakad av hypofystumörer.

ACKNOWLEDGEMENT

This thesis would not have been possible without the contributions of several people with a wide range of professional backgrounds and expertise. For me, the opportunity to meet, cooperate with and learn from all these people have been the most valued aspect of my doctoral studies.

First, I would like to thank my supervisor, **Daniel Nilsson**, for giving me this opportunity, for generously sharing both clinical and research experiences with me and for encouraging me all along my studies. His ability to combine clinical work and research with the patient's best interest in focus has been a true inspiration.

I thank my co-supervisors, **Thomas Skoglund**, **Henrik Bergquist** and **Håkan Olausson**, for their support and wise remarks that have contributed to a sound perspective on the research.

Maria Ljungberg and **Göran Starck**, MRI physicists and valued research colleagues, have been my unofficial supervisors, accepting all my questions – high and low – and always considering them with a contagious enthusiasm for their field.

Thank you, **Oscar Gustafsson**, MRI physicist, for an inspiring companionship, including long discussions and endless e-mail conversations!

Thank you, professors **Kristina Malmgren** and **Bertil Rydenhag** of the epilepsy team, for your invaluable expertise and encouragement.

Thank you, professors of neuro-ophthalmology, **Bertil Lindblom** and **Lars Frisén**, for your generous and patient cooperation, essential for this thesis.

All the people at MedTechWest, including director **Henrik Mindedal**, have provided a peaceful and inspiring research environment throughout my studies – thank you for including me in your community!

I would like to thank the research nurses who have participated and made the studies possible. Special thanks to **Rose-Marie Rang** at the neuro-ophthalmology department, for friendly cooperation throughout all the studies.

Thank you to all my competent colleagues at the ENT clinic who have been a source of inspiration as well as a constant friendly support. **Nina Pauli**, thank you for your excellent “roommateship”!

Thank you, neurosurgeons at Sahlgrenska, for including me in your circle. Special thanks to **Karl-Erik Jakobsson**, for cooperation and encouragement.

Thank you, **Dr. Joseph Wu** at UCI, California, for introducing me to the field of neuroimaging and for giving me the opportunity to accompany you in all aspects of your research.

I would like to thank all my friends and family for their interest and encouragement. I especially thank my parents, **Eva-Britt** and **Kaj**, for making me believe I can do anything I want, which has lead to so many adventures in my life, including this thesis. Thank you, pappa, for the gift of curiosity!

Thomas, thank you for taking part in all of my work with commitment and patience and, above all, thank you for being my home.

Lastly, I would like to thank all the patients who have generously agreed to participate and made the studies possible.

REFERENCES

1. Anastasopoulos C, Reisert M, Kiselev VG, Nguyen-Thanh T, Schulze-Bonhage A, Zentner J, et al: Local and global fiber tractography in patients with epilepsy. **AJNR Am J Neuroradiol 35:**291-296, 2014
2. Archambault L: Le faisceau longitudinal inferieur et le faisceau optique central: Quelques considerations sur les fibres d´association du cerveau. **Rev Neurol 4:**1206, 1906
3. Ashburner J, Friston KJ: Voxel-based morphometry--the methods. **Neuroimage 11:**805-821, 2000
4. Basser PJ, Mattiello J, LeBihan D: Estimation of the effective self-diffusion tensor from the NMR spin echo. **J Magn Reson B 103:**247-254, 1994
5. Basser PJ, Mattiello J, LeBihan D: MR diffusion tensor spectroscopy and imaging. **Biophys J 66:**259-267, 1994
6. Basser PJ, Pajevic S, Pierpaoli C, Duda J, Aldroubi A: In vivo fiber tractography using DT-MRI data. **Magn Reson Med 44:**625-632, 2000
7. Beaulieu C: The basis of anisotropic water diffusion in the nervous system - a technical review. **NMR Biomed 15:**435-455, 2002
8. Beaulieu C, Allen PS: Determinants of anisotropic water diffusion in nerves. **Magn Reson Med 31:**394-400, 1994
9. Beaulieu C, Allen PS: Water diffusion in the giant axon of the squid: implications for diffusion-weighted MRI of the nervous system. **Magn Reson Med 32:**579-583, 1994
10. Behrens TE, Berg HJ, Jbabdi S, Rushworth MF, Woolrich MW: Probabilistic diffusion tractography with multiple fibre orientations: What can we gain? **Neuroimage 34:**144-155, 2007
11. Behrens TE, Woolrich MW, Jenkinson M, Johansen-Berg H, Nunes RG, Clare S, et al: Characterization and propagation of uncertainty in diffusion-weighted MR imaging. **Magn Reson Med 50:**1077-1088, 2003
12. Bisdas S, Bohning DE, Besenski N, Nicholas JS, Rumboldt Z: Reproducibility, interrater agreement, and age-related changes of fractional anisotropy measures at 3T in healthy subjects: effect of the applied b-value. **AJNR Am J Neuroradiol 29:**1128-1133, 2008
13. Bjellvi J, Flink R, Rydenhag B, Malmgren K: Complications of epilepsy surgery in Sweden 1996-2010: a prospective, population-based study. **J Neurosurg 122:**519-525, 2015
14. Bjellvi J, Rydenhag B, Malmgren K: Visual field defects and permission to drive in adults after temporal lobe resections for epilepsy. **Epilepsia:**4-246, 2014

15. Bonekamp D, Nagae LM, Degaonkar M, Matson M, Abdalla WM, Barker PB, et al: Diffusion tensor imaging in children and adolescents: reproducibility, hemispheric, and age-related differences. **Neuroimage 34:**733-742, 2007
16. Borius PY, Roux FE, Valton L, Sol JC, Lotterie JA, Berry I: Can DTI fiber tracking of the optic radiations predict visual deficit after surgery? **Clin Neurol Neurosurg 122:**87-91, 2014
17. Brander A, Kataja A, Saastamoinen A, Ryymin P, Huhtala H, Ohman J, et al: Diffusion tensor imaging of the brain in a healthy adult population: Normative values and measurement reproducibility at 3 T and 1.5 T. **Acta Radiol 51:**800-807, 2010
18. Brodal P: The central nervous system: structure and function, in**, ed 4th.** New York: Oxford University Press, 2010
19. Brown R: A brief account of microscopic observations made on the particles contained in the pollen of plants. **London and Edinburgh philosophical magazine and journal of science 4:**161-173, 1828
20. Carrim ZI, Reeks GA, Chohan AW, Dunn LT, Hadley DM: Predicting impairment of central vision from dimensions of the optic chiasm in patients with pituitary adenoma. **Acta Neurochir (Wien) 149:**255-260; discussion 260, 2007
21. Catani M, Howard RJ, Pajevic S, Jones DK: Virtual in vivo interactive dissection of white matter fasciculi in the human brain. **Neuroimage 17:**77-94, 2002
22. Chauhan BC, House PH, McCormick TA, LeBlanc RP: Comparison of conventional and high-pass resolution perimetry in a prospective study of patients with glaucoma and healthy controls. **Arch Ophthalmol 117:**24-33, 1999
23. Chen X, Weigel D, Ganslandt O, Buchfelder M, Nimsky C: Prediction of visual field deficits by diffusion tensor imaging in temporal lobe epilepsy surgery. **Neuroimage 45:**286-297, 2009
24. Chowdhury FH, Khan AH: Anterior & lateral extension of optic radiation & safety of amygdalohippocampectomy through middle temporal gyrus: a cadaveric study of 11 cerebral hemispheres. **Asian J Neurosurg 5:**78-82, 2010
25. Conturo TE, Lori NF, Cull TS, Akbudak E, Snyder AZ, Shimony JS, et al: Tracking neuronal fiber pathways in the living human brain. **Proc Natl Acad Sci U S A 96:**10422-10427, 1999
26. Cottee LJ, Daniel C, Loh WS, Harrison BM, Burke W: Remyelination and recovery of conduction in cat optic nerve after demyelination by pressure. **Exp Neurol 184:**865-877, 2003
27. Danesh-Meyer HV, Wong A, Papchenko T, Matheos K, Stylli S, Nichols A, et al: Optical coherence tomography predicts visual outcome for pituitary tumors. **J Clin Neurosci 22:**1098-1104, 2015
28. Dasenbrock HH, Smith SA, Ozturk A, Farrell SK, Calabresi PA, Reich DS: Diffusion tensor imaging of the optic tracts in multiple

sclerosis: association with retinal thinning and visual disability. **J Neuroimaging 21:**e41-49, 2011
29. Descoteaux M, Angelino E, Fitzgibbons S, Deriche R: Regularized, fast, and robust analytical Q-ball imaging. **Magn Reson Med 58:**497-510, 2007
30. Dreessen de Gervai P, Sboto-Frankenstein UN, Bolster RB, Thind S, Gruwel ML, Smith SD, et al: Tractography of Meyer's Loop asymmetries. **Epilepsy Res 108:**872-882, 2014
31. Dyrby TB, Sogaard LV, Parker GJ, Alexander DC, Lind NM, Baare WF, et al: Validation of in vitro probabilistic tractography. **Neuroimage 37:**1267-1277, 2007
32. Ebeling U, Reulen HJ: Neurosurgical topography of the optic radiation in the temporal lobe. **Acta Neurochir (Wien) 92:**29-36, 1988
33. Edal AL, Skjodt K, Nepper-Rasmussen HJ: SIPAP--a new MR classification for pituitary adenomas. Suprasellar, infrasellar, parasellar, anterior and posterior. **Acta Radiol 38:**30-36, 1997
34. Egan RA, Shults WT, So N, Burchiel K, Kellogg JX, Salinsky M: Visual field deficits in conventional anterior temporal lobectomy versus amygdalohippocampectomy. **Neurology 55:**1818-1822, 2000
35. Einstein A: Über die von der molekularkinetischen Theorie der Wärme geforderte Bewegung von in ruhenden Flüssigkeiten suspendierten Teilchen. **Annalen der Physik 322:**549-560, 1905
36. Ezzat S, Asa SL, Couldwell WT, Barr CE, Dodge WE, Vance ML, et al: The prevalence of pituitary adenomas: a systematic review. **Cancer 101:**613-619, 2004
37. Fleiss J: **Design and Analysis of Clinical Experiments.** New York: John Wiley & Sons, 1986
38. Foroozan R: Chiasmal syndromes. **Curr Opin Ophthalmol 14:**325-331, 2003
39. Frisen L: High-pass resolution perimetry. A clinical review. **Doc Ophthalmol 83:**1-25, 1993
40. Frisen L: High-pass resolution targets in peripheral vision. **Ophthalmology 94:**1104-1108, 1987
41. Frisen L, Jensen C: How robust is the optic chiasm? Perimetric and neuro-imaging correlations. **Acta Neurol Scand 117:**198-204, 2008
42. Good CD, Johnsrude IS, Ashburner J, Henson RN, Friston KJ, Frackowiak RS: A voxel-based morphometric study of ageing in 465 normal adult human brains. **Neuroimage 14:**21-36, 2001
43. Grech-Sollars M, Hales PW, Miyazaki K, Raschke F, Rodriguez D, Wilson M, et al: Multi-centre reproducibility of diffusion MRI parameters for clinical sequences in the brain. **NMR Biomed 28:**468-485, 2015

44. Gulani V, Webb AG, Duncan ID, Lauterbur PC: Apparent diffusion tensor measurements in myelin-deficient rat spinal cords. **Magn Reson Med 45:**191-195, 2001
45. Hakulinen U, Brander A, Ryymin P, Ohman J, Soimakallio S, Helminen M, et al: Repeatability and variation of region-of-interest methods using quantitative diffusion tensor MR imaging of the brain. **BMC Med Imaging 12:**30, 2012
46. Halvorsen H, Ramm-Pettersen J, Josefsen R, Ronning P, Reinlie S, Meling T, et al: Surgical complications after transsphenoidal microscopic and endoscopic surgery for pituitary adenoma: a consecutive series of 506 procedures. **Acta Neurochir (Wien) 156:**441-449, 2014
47. Harrington DO: Visual field character in temporal and occipital lobe lesions. Localizing values of congruity and incogruity in incomplete homonymous hemianopsia. **Arch Ophthalmol 66:**778-792, 1961
48. Jakobsson KE, Petruson B, Lindblom B: Dynamics of visual improvement following chiasmal decompression. Quantitative pre- and postoperative observations. **Acta Ophthalmol Scand 80:**512-516, 2002
49. James JS, Radhakrishnan A, Thomas B, Madhusoodanan M, Kesavadas C, Abraham M, et al: Diffusion tensor imaging tractography of Meyer's loop in planning resective surgery for drug-resistant temporal lobe epilepsy. **Epilepsy Res 110:**95-104, 2015
50. Jeelani NU, Jindahra P, Tamber MS, Poon TL, Kabasele P, James-Galton M, et al: 'Hemispherical asymmetry in the Meyer's Loop': a prospective study of visual-field deficits in 105 cases undergoing anterior temporal lobe resection for epilepsy. **J Neurol Neurosurg Psychiatry 81:**985-991, 2010
51. Jenkinson M, Smith S: A global optimisation method for robust affine registration of brain images. **Med Image Anal 5:**143-156, 2001
52. Johansson C, Lindblom B: The role of optical coherence tomography in the detection of pituitary adenoma. **Acta Ophthalmol 87:**776-779, 2009
53. Jonas JB, Schmidt AM, Muller-Bergh JA, Schlotzer-Schrehardt UM, Naumann GO: Human optic nerve fiber count and optic disc size. **Invest Ophthalmol Vis Sci 33:**2012-2018, 1992
54. Jones DK: Studying connections in the living human brain with diffusion MRI. **Cortex 44:**936-952, 2008
55. Jones DK, Cercignani M: Twenty-five pitfalls in the analysis of diffusion MRI data. **NMR Biomed 23:**803-820, 2010
56. Jovicich J, Marizzoni M, Bosch B, Bartres-Faz D, Arnold J, Benninghoff J, et al: Multisite longitudinal reliability of tract-based spatial statistics in diffusion tensor imaging of healthy elderly subjects. **Neuroimage 101:**390-403, 2014

57. Kerrison JB, Lynn MJ, Baer CA, Newman SA, Biousse V, Newman NJ: Stages of improvement in visual fields after pituitary tumor resection, in **Am J Ophthalmol, ed 2000/12/22**, 2000, Vol 130, pp 813-820
58. Knosche TR, Anwander A, Liptrot M, Dyrby TB: Validation of tractography: Comparison with manganese tracing. **Hum Brain Mapp 36:**4116-4134, 2015
59. Kristof RA, Kirchhofer D, Handzel D, Neuloh G, Schramm J, Mueller CA, et al: Pre-existing chiasma syndromes do not entirely remit following transsphenoidal surgery for pituitary adenomas. **Acta Neurochir (Wien) 153:**26-32, 2011
60. Lee CE, Danielian LE, Thomasson D, Baker EH: Normal regional fractional anisotropy and apparent diffusion coefficient of the brain measured on a 3 T MR scanner. **Neuroradiology 51:**3-9, 2009
61. Lilja Y, Ljungberg M, Starck G, Malmgren K, Rydenhag B, Nilsson DT: Visualizing Meyer's loop: A comparison of deterministic and probabilistic tractography. **Epilepsy Res 108:**481-490, 2014
62. Lim JC, Phal PM, Desmond PM, Nichols AD, Kokkinos C, Danesh-Meyer HV, et al: Probabilistic MRI tractography of the optic radiation using constrained spherical deconvolution: a feasibility study. **PLoS One 10:**e0118948, 2015
63. Ludwig K: **Atlas Cerebri Humani**: Karger, Basel, 1956
64. Magnotta VA, Matsui JT, Liu D, Johnson HJ, Long JD, Bolster BD, Jr., et al: Multicenter reliability of diffusion tensor imaging. **Brain Connect 2:**345-355, 2012
65. Manji H, T PG: Epilepsy surgery, visual fields, and driving: a study of the visual field criteria for driving in patients after temporal lobe epilepsy surgery with a comparison of Goldmann and Esterman perimetry. **J Neurol Neurosurg Psychiatry 68:**80-82, 2000
66. Meyer A: The connections of the occipital lobes and the present status of the cerebral visual affections. **Trans Assoc Am Physicians 22:**7-16, 1907
67. Mori S, Crain BJ, Chacko VP, van Zijl PC: Three-dimensional tracking of axonal projections in the brain by magnetic resonance imaging. **Ann Neurol 45:**265-269, 1999
68. Mori S, van Zijl PC: Fiber tracking: principles and strategies - a technical review. **NMR Biomed 15:**468-480, 2002
69. Mori S, Zhang J: Principles of diffusion tensor imaging and its applications to basic neuroscience research. **Neuron 51:**527-539, 2006
70. Moritani T, Ekholm S, Westesson P (eds): **Diffusion-Weighted MR Imaging of the Brain, ed Second Edition**, 2009
71. Moseley ME, Cohen Y, Kucharczyk J, Mintorovitch J, Asgari HS, Wendland MF, et al: Diffusion-weighted MR imaging of anisotropic

water diffusion in cat central nervous system. **Radiology 176:**439-445, 1990

72. Nguyen TH, Yoshida M, Stievenart JL, Iba-Zizen MT, Bellinger L, Abanou A, et al: MR tractography with diffusion tensor imaging in clinical routine. **Neuroradiology 47:**334-343, 2005
73. Nilsson D, Malmgren K, Rydenhag B, Frisen L: Visual field defects after temporal lobectomy -- comparing methods and analysing resection size. **Acta Neurol Scand 110:**301-307, 2004
74. Nilsson D, Starck G, Ljungberg M, Ribbelin S, Jonsson L, Malmgren K, et al: Intersubject variability in the anterior extent of the optic radiation assessed by tractography. **Epilepsy Res 77:**11-16, 2007
75. Nimsky C, Ganslandt O, Fahlbusch R: Implementation of fiber tract navigation. **Neurosurgery 58:**ONS-292-303; discussion ONS-303-294, 2006
76. Nimsky C, Ganslandt O, Hastreiter P, Wang R, Benner T, Sorensen AG, et al: Preoperative and intraoperative diffusion tensor imaging-based fiber tracking in glioma surgery. **Neurosurgery 56:**130-137; discussion 138, 2005
77. Ozturk A, Sasson AD, Farrell JA, Landman BA, da Motta AC, Aralasmak A, et al: Regional differences in diffusion tensor imaging measurements: assessment of intrarater and interrater variability. **AJNR Am J Neuroradiol 29:**1124-1127, 2008
78. Parravano JG, Toledo A, Kucharczyk W: Dimensions of the optic nerves, chiasm, and tracts: MR quantitative comparison between patients with optic atrophy and normals. **J Comput Assist Tomogr 17:**688-690, 1993
79. Pathak-Ray V, Ray A, Walters R, Hatfield R: Detection of visual field defects in patients after anterior temporal lobectomy for mesial temporal sclerosis-establishing eligibility to drive. **Eye (Lond) 16:**744-748, 2002
80. Paul DA, Gaffin-Cahn E, Hintz EB, Adeclat GJ, Zhu T, Williams ZR, et al: White matter changes linked to visual recovery after nerve decompression. **Sci Transl Med 6:**266ra173, 2014
81. Petruson B, Jakobsson KE, Elfverson J, Bengtsson BA: Five-year follow-up of nonsecreting pituitary adenomas. **Arch Otolaryngol Head Neck Surg 121:**317-322, 1995
82. Peuskens D, van Loon J, Van Calenbergh F, van den Bergh R, Goffin J, Plets C: Anatomy of the anterior temporal lobe and the frontotemporal region demonstrated by fiber dissection. **Neurosurgery 55:**1174-1184, 2004
83. Powell HW, Parker GJ, Alexander DC, Symms MR, Boulby PA, Wheeler-Kingshott CA, et al: MR tractography predicts visual field defects following temporal lobe resection. **Neurology 65:**596-599, 2005

84. Powell M: Recovery of vision following transsphenoidal surgery for pituitary adenomas. **Br J Neurosurg 9:**367-373, 1995
85. Rubino PA, Rhoton AL, Jr., Tong X, Oliveira E: Three-dimensional relationships of the optic radiation. **Neurosurgery 57:**219-227; discussion 219-227, 2005
86. Schmalisch K, Milian M, Schimitzek T, Lagreze WA, Honegger J: Predictors for visual dysfunction in nonfunctioning pituitary adenomas - implications for neurosurgical management. **Clin Endocrinol (Oxf) 77:**728-734, 2012
87. Schulz G, Crooijmans HJ, Germann M, Scheffler K, Muller-Gerbl M, Muller B: Three-dimensional strain fields in human brain resulting from formalin fixation. **J Neurosci Methods 202:**17-27, 2011
88. Semah F, Ryvlin P: Can we predict refractory epilepsy at the time of diagnosis? **Epileptic Disord 7 Suppl 1:**S10-13, 2005
89. Sherbondy AJ, Dougherty RF, Napel S, Wandell BA: Identifying the human optic radiation using diffusion imaging and fiber tractography. **J Vis 8:**12 11-11, 2008
90. Smith SM, Jenkinson M, Johansen-Berg H, Rueckert D, Nichols TE, Mackay CE, et al: Tract-based spatial statistics: voxelwise analysis of multi-subject diffusion data. **Neuroimage 31:**1487-1505, 2006
91. Song SK, Sun SW, Ju WK, Lin SJ, Cross AH, Neufeld AH: Diffusion tensor imaging detects and differentiates axon and myelin degeneration in mouse optic nerve after retinal ischemia. **Neuroimage 20:**1714-1722, 2003
92. Song SK, Yoshino J, Le TQ, Lin SJ, Sun SW, Cross AH, et al: Demyelination increases radial diffusivity in corpus callosum of mouse brain. **Neuroimage 26:**132-140, 2005
93. Stejskal E, Tanner J: Spin diffusion measurements: Spin echoes in the presence of a time-dependent field gradient. **Journal of Chemical Physics 42:**288-292, 1965
94. Stieltjes B, Kaufmann WE, van Zijl PC, Fredericksen K, Pearlson GD, Solaiyappan M, et al: Diffusion tensor imaging and axonal tracking in the human brainstem. **Neuroimage 14:**723-735, 2001
95. Tabaee A, Anand VK, Barron Y, Hiltzik DH, Brown SM, Kacker A, et al: Endoscopic pituitary surgery: a systematic review and meta-analysis. **J Neurosurg 111:**545-554, 2009
96. Takahashi M, Hackney DB, Zhang G, Wehrli SL, Wright AC, O'Brien WT, et al: Magnetic resonance microimaging of intraaxonal water diffusion in live excised lamprey spinal cord. **Proc Natl Acad Sci U S A 99:**16192-16196, 2002
97. Taoka T, Sakamoto M, Nakagawa H, Nakase H, Iwasaki S, Takayama K, et al: Diffusion Tensor Tractography of the Meyer Loop in Cases of Temporal Lobe Resection for Temporal Lobe Epilepsy: Correlation Between Postsurgical Visual Field Defect and

Anterior Limit of Meyer Loop on Tractography. **AJNR Am J Neuroradiol**, 2008
98. Taylor DC, McMacKin D, Staunton H, Delanty N, Phillips J: Patients' aims for epilepsy surgery: desires beyond seizure freedom. **Epilepsia 42:**629-633, 2001
99. Thomas C, Ye FQ, Irfanoglu MO, Modi P, Saleem KS, Leopold DA, et al: Anatomical accuracy of brain connections derived from diffusion MRI tractography is inherently limited. **Proc Natl Acad Sci U S A 111:**16574-16579, 2014
100. Thudium MO, Campos AR, Urbach H, Clusmann H: The basal temporal approach for mesial temporal surgery: sparing the Meyer loop with navigated diffusion tensor tractography. **Neurosurgery 67:**385-390, 2010
101. Tournier JD, Calamante F, Connelly A: MRtrix: Diffusion tractography in crossing fiber regions. **International JOurnal of Imaging systems and technology 22:**53-66, 2012
102. Tournier JD, Calamante F, Connelly A: Robust determination of the fibre orientation distribution in diffusion MRI: non-negativity constrained super-resolved spherical deconvolution. **Neuroimage 35:**1459-1472, 2007
103. Trip SA, Wheeler-Kingshott C, Jones SJ, Li WY, Barker GJ, Thompson AJ, et al: Optic nerve diffusion tensor imaging in optic neuritis. **Neuroimage 30:**498-505, 2006
104. Veenith TV, Carter E, Grossac J, Newcombe VF, Outtrim JG, Lupson V, et al: Inter subject variability and reproducibility of diffusion tensor imaging within and between different imaging sessions. **PLoS One 8:**e65941, 2013
105. Vollmar C, O'Muircheartaigh J, Barker GJ, Symms MR, Thompson P, Kumari V, et al: Identical, but not the same: intra-site and inter-site reproducibility of fractional anisotropy measures on two 3.0T scanners. **Neuroimage 51:**1384-1394, 2010
106. Wang H, Sun W, Fu Z, Si Z, Zhu Y, Zhai G, et al: The pattern of visual impairment in patients with pituitary adenoma. **J Int Med Res 36:**1064-1069, 2008
107. Wang JY, Abdi H, Bakhadirov K, Diaz-Arrastia R, Devous MD, Sr.: A comprehensive reliability assessment of quantitative diffusion tensor tractography. **Neuroimage 60:**1127-1138, 2012
108. Wiebe S, Blume WT, Girvin JP, Eliasziw M: A randomized, controlled trial of surgery for temporal-lobe epilepsy. **N Engl J Med 345:**311-318, 2001
109. Wilkins B, Lee N, Gajawelli N, Law M, Lepore N: Fiber estimation and tractography in diffusion MRI: development of simulated brain images and comparison of multi-fiber analysis methods at clinical b-values. **Neuroimage 109:**341-356, 2015

110. Winston GP, Daga P, Stretton J, Modat M, Symms MR, McEvoy AW, et al: Optic radiation tractography and vision in anterior temporal lobe resection. **Ann Neurol 71:**334-341, 2012
111. Winston GP, Daga P, White MJ, Micallef C, Miserocchi A, Mancini L, et al: Preventing visual field deficits from neurosurgery. **Neurology 83:**604-611, 2014
112. Winston GP, Mancini L, Stretton J, Ashmore J, Symms MR, Duncan JS, et al: Diffusion tensor imaging tractography of the optic radiation for epilepsy surgical planning: a comparison of two methods. **Epilepsy Res 97:**124-132, 2011
113. Woolrich MW, Jbabdi S, Patenaude B, Chappell M, Makni S, Behrens T, et al: Bayesian analysis of neuroimaging data in FSL. **Neuroimage 45:**S173-186, 2009
114. Xu J, Sun SW, Naismith RT, Snyder AZ, Cross AH, Song SK: Assessing optic nerve pathology with diffusion MRI: from mouse to human. **NMR Biomed 21:**928-940, 2008
115. Yamamoto T, Yamada K, Nishimura T, Kinoshita S: Tractography to depict three layers of visual field trajectories to the calcarine gyri. **Am J Ophthalmol 140:**781-785, 2005
116. Yanoff M, Duker J (eds): **Ophthalmology, ed 3rd**: Elsevier, 2009
117. Yogarajah M, Focke NK, Bonelli S, Cercignani M, Acheson J, Parker GJ, et al: Defining Meyer's loop-temporal lobe resections, visual field deficits and diffusion tensor tractography. **Brain 132:**1656-1668, 2009
118. Zhang YQ, Li J, Xu L, Zhang L, Wang ZC, Yang H, et al: Anterior visual pathway assessment by magnetic resonance imaging in normal-pressure glaucoma. **Acta Ophthalmol 90:**e295-302, 2012